



National Library  
of Canada

Acquisitions and  
Bibliographic Services Branch

395 Wellington Street  
Ottawa, Ontario  
K1A 0N4

Bibliothèque nationale  
du Canada

Direction des acquisitions et  
des services bibliographiques

395, rue Wellington  
Ottawa (Ontario)  
K1A 0N4

*Your file - Votre référence*

*Our file - Notre référence*

## NOTICE

The quality of this microform is heavily dependent upon the quality of the original thesis submitted for microfilming. Every effort has been made to ensure the highest quality of reproduction possible.

If pages are missing, contact the university which granted the degree.

Some pages may have indistinct print especially if the original pages were typed with a poor typewriter ribbon or if the university sent us an inferior photocopy.

Reproduction in full or in part of this microform is governed by the Canadian Copyright Act, R.S.C. 1970, c. C-30, and subsequent amendments.

## AVIS

La qualité de cette microforme dépend grandement de la qualité de la thèse soumise au microfilmage. Nous avons tout fait pour assurer une qualité supérieure de reproduction.

S'il manque des pages, veuillez communiquer avec l'université qui a conféré le grade.

La qualité d'impression de certaines pages peut laisser à désirer, surtout si les pages originales ont été dactylographiées à l'aide d'un ruban usé ou si l'université nous a fait parvenir une photocopie de qualité inférieure.

La reproduction, même partielle, de cette microforme est soumise à la Loi canadienne sur le droit d'auteur, SRC 1970, c. C-30, et ses amendements subséquents.

# **Fabrication of Three Dimensional Micro-Structures by Localized Electrochemical Deposition**

by  
**John David Wyndham Madden**

A Thesis submitted to the  
Faculty of Graduate Studies and Research  
in partial fulfillment of the requirements of the degree of  
Master of Engineering

**Biorobotics Laboratory  
Department of Biomedical Engineering  
McGill University  
Montréal, Québec, Canada  
November, 1994**

**Copyright John David Wyndham Madden, 1994**



National Library  
of Canada

Acquisitions and  
Bibliographic Services Branch

395 Wellington Street  
Ottawa, Ontario  
K1A 0N4

Bibliothèque nationale  
du Canada

Direction des acquisitions et  
des services bibliographiques

395, rue Wellington  
Ottawa (Ontario)  
K1A 0N4

*Your file* *Votre référence*

*Our file* *Notre référence*

THE AUTHOR HAS GRANTED AN IRREVOCABLE NON-EXCLUSIVE LICENCE ALLOWING THE NATIONAL LIBRARY OF CANADA TO REPRODUCE, LOAN, DISTRIBUTE OR SELL COPIES OF HIS/HER THESIS BY ANY MEANS AND IN ANY FORM OR FORMAT, MAKING THIS THESIS AVAILABLE TO INTERESTED PERSONS.

L'AUTEUR A ACCORDE UNE LICENCE IRREVOCABLE ET NON EXCLUSIVE PERMETTANT A LA BIBLIOTHEQUE NATIONALE DU CANADA DE REPRODUIRE, PRETER, DISTRIBUER OU VENDRE DES COPIES DE SA THESE DE QUELQUE MANIERE ET SOUS QUELQUE FORME QUE CE SOIT POUR METTRE DES EXEMPLAIRES DE CETTE THESE A LA DISPOSITION DES PERSONNE INTERESSEES.

THE AUTHOR RETAINS OWNERSHIP OF THE COPYRIGHT IN HIS/HER THESIS. NEITHER THE THESIS NOR SUBSTANTIAL EXTRACTS FROM IT MAY BE PRINTED OR OTHERWISE REPRODUCED WITHOUT HIS/HER PERMISSION.

L'AUTEUR CONSERVE LA PROPRIETE DU DROIT D'AUTEUR QUI PROTEGE SA THESE. NI LA THESE NI DES EXTRAITS SUBSTANTIELS DE CELLE-CI NE DOIVENT ETRE IMPRIMES OU AUTREMENT REPRODUITS SANS SON AUTORISATION.

ISBN 0-612-05460-8

**Canada**

## Abstract

A new microfabrication technology capable of electro-depositing truly three dimensional metal micro-structures is presented. The method, known as Spatially Constrained Micro-Electro-Deposition or SCMED, is being developed as part of an effort to provide sub-millimeter sized tools and extra degrees of freedom to existing tele-operated micro-surgical robots and micro-manipulators. These applications require fabrication processes capable of producing three dimensional structures, with sub-micrometer spatial resolution, using a range of materials and at reasonable rates. Current micro-fabrication technology is unable to meet these requirements. The three dimensional requirement is particularly relevant given the present dependence on essentially two dimensional micro-fabrication methods derived from micro-electronics.

In SCMED, electrodeposition is localized by placing a sharp tipped electrode in a plating solution, near a substrate, and applying a voltage. Structures are built by moving the electrode appropriately with respect to the substrate.

Electrochemical theory, including mass transport to regions of localized field, is discussed, and a model of deposition profile presented. SCMED is shown to be capable of producing three dimensional polycrystalline nickel structures on the micrometer scale, including a multi-coiled helical spring. Vertical deposition rates of  $6 \mu\text{m/s}$  are observed, two orders of magnitude greater than those of conventional electrodeposition.

The process can potentially deposit and etch a wide range of materials including pure metals, alloys and polymers with sub-micrometer resolution, thereby overcoming important limitations of current technology.

## Résumé

Une nouvelle méthode de microfabrication pouvant effectuer de l'électro-déposition de micro-structures métalliques tri-dimensionnelles est présentée. La méthode, nommé SCMED (Spatially Constrained Micro-Electro-Deposition ou la Micro-Electrodéposition Spatialement Localisée), est requise pour la construction de petits outils ( $<1\text{mm}$ ) et pour l'addition de degrés de liberté supplémentaires à des robots de microchirurgie et des micro-manipulateurs télé-opérés. Ces applications ont besoin de méthodes de fabrication capable de construire des structures tri-dimensionnelles, avec une résolution supérieure au micromètre, utilisant divers matériaux et fonctionnant à des vitesses raisonnables. Présentement la technologie ne peut pas satisfaire ces besoins et les méthodes les plus communes produisent essentiellement des patrons en deux dimensions.

SCMED localise l'électrodéposition en localisant le champ électrique. Ceci est accompli en utilisant une électrode pointue placée près de la surface où la déposition est requise, dans une solution d'électro-plaquage, et en appliquant une tension électrique. Les structures sont fabriquées en bougeant en trois dimensions la pointe de l'électrode par rapport à la surface.

La théorie électrochimique est présentée, incluant une discussion des effets de transport de masse jusqu'aux régions de déposition localisée et un modèle du profil du champ électrique. Il est démontré que la technique de SCMED peut produire des micro-structures tri-dimensionnelles poly-cristallines en nickel, tel un ressort hélicoïdal. Des vitesses de déposition verticale de  $6\ \mu\text{m/s}$  sont observées avec la technique de SCMED, dépassant la vitesse de l'électrodéposition conventionnelle par plus de deux ordres de magnitude.

Le procédé peut potentiellement déposer plusieurs matériaux incluant des métaux purs, des alliages et des polymères avec une résolution supérieure au micromètre, surmontant des limitations importantes qui se présentent avec la technologie courante.

## Preface

This thesis describes the development of a new micro-fabrication process known as Spatially Constrained Micro-Electrochemical Deposition, or SCMED. The SCMED concept was first proposed by Professor Ian Hunter. My task was implement the idea and determine its feasibility. The thesis serves both to fulfill a master's degree requirement and as a reference source for the use and further development of SCMED. I also hope to provide the reader with some insight into the current state of micro- and nano-technology and its present limitations, and thereby to demonstrate the need for a new approach to fabrication, such as SCMED.

The work described represents the evolution of SCMED from its conception to a level of performance very similar to those of other fabrication methods in its class. Efforts are underway to improve resolution by two orders of magnitude and to enable construction of integrated metal and polymer micro-structures. If successful, the accomplishment will be a major step towards the fabrication of sub-millimeter sized autonomous robots, among other applications.

Research was carried out in the Biorobotics Laboratory in the Department of Biomedical Engineering at McGill University and in the Department of Mechanical Engineering at the Massachusetts Institute of Technology, where it continues.

I would like to thank my supervisor, Professor Ian Hunter, for his help and guidance. His vision and enthusiasm, coupled with his very broad scientific knowledge and experience, create an extremely stimulating learning environment.

Thanks to Colin Brennan for the many discussions that have helped solidify my understanding of the design issues and provided new insights. I am also grateful for his rigorous evaluation of my work. Serge Lafontaine's help and patience with my many queries regarding electronics and computing are greatly appreciated. I would also like to thank Peter Mad-

den for his collaboration in the development of software for controlling the stepping motors and in the etching of electrodes.

My parents, Dr. John C. and Sidney Madden, have supported and encouraged me in this work and throughout my life, for which I am very grateful.

Finally, the financial support of the National Science and Engineering Research Council of Canada through a Post Graduate Scholarship is much appreciated.

# Table of Contents

Abstract	i
Résumé	ii
Preface	iii
Table of Contents	v
List of Figures	viii
List of Tables	ix
<b>CHAPTER ONE: Introduction and Design Philosophy</b>	<b>1</b>
1. Opportunities in Nanotechnology	3
2. Nature – A View into the Future?	6
3. Biotechnology and Fabrication	7
4. Effects of Scaling	9
5. Downward Engineering – From Macro to Micro	10
<b>CHAPTER TWO: Overview of Micro-Fabrication Technology</b>	<b>12</b>
1. Material Removal	12
2. Material Addition	13
3. Fabrication Techniques	14
1. Conventional Fabrication	16
2. Photo-Lithography and Related Methods	16
1. Photo-Lithography	16
2. LIGA and High Aspect Ratio Lithography	17
3. Material Removal Methods	18
1. Excimer Laser Ablation	18
2. Ion Milling	19
3. Electron Beam Milling	20
4. Electrical Discharge Machining (EDM)	20
4. Material Addition Methods	21
1. Stereo Lithography	21
2. Powder Deposition	22
3. Laser Assisted Chemical Vapour Deposition (LCVD)	22

5. Scanning Tunneling Microscopy (STM)	23
6. Electrochemical Methods	24
1. Electroless Plating	24
2. Laser Enhanced Electro-Plating (LEEP)	25
3. Scanning Electrochemical Microscopy (SECM)	26
7. Summary	27
<b>CHAPTER THREE: Electrochemical Theory</b>	<b>29</b>
1. Concept of SCMED	29
2. Deposition Rate	29
1. Electron Transfer	30
2. Mass Transport	31
1. Diffusion	31
2. Convection	32
3. Migration	33
4. Electro-Crystallization	34
3. Deposition Profile	35
3. Summary of Theory	38
<b>CHAPTER FOUR: The Forced Convection Approach</b>	<b>39</b>
1. SCMED Deposition and Forced Convection	39
1. Implementation	40
2. Scaling Effects	41
1. Model of Pressure Drop in Flow through a Pipette	41
2. Electrical Resistance and Potential Drop	44
3. Deposition Control	46
4. Magneto-Hydrodynamic Flow	47
5. Deposition without Forced Convection	48
<b>CHAPTER FIVE: Experimental Methods</b>	<b>49</b>

CHAPTER SIX: Results	51
1. Nickel Structures	51
2. Material Properties	52
i. Spring Constant and Modulus of Elasticity	52
2. X-ray Crystallography	53
3. Measuring Conductivity	54
1. Theory	54
2. Apparatus and Procedure	56
3. Results	58
CHAPTER SEVEN: Discussion and Future Work	59
1. Resolution	61
2. Control	62
3. Surface Finish	63
4. Materials	63
5. Underlying Mechanisms	64
6. Machining and Alterations	65
7. A Micro-Fabrication Centre	65
Conclusion	66
References	67

## List of Figures

<b>Figure 1:</b>	“There’s Plenty of Room at the Bottom”	6
<b>Figure 2:</b>	Fabrication Rate and Resolution of 3D Technologies	27
<b>Figure 3(a):</b>	The SCMED Concept	29
<b>Figure 3(b):</b>	Creating of a Structure using SCMED	29
<b>Figure 4:</b>	Modelled Electrode Tip Geometries	36
<b>Figure 5:</b>	Modelled Cross–Section of Current Density between a Disk and a Planar Substrate	37
<b>Figure 6:</b>	Modelled Magnitude of Electric Field at the Substrate Surface	37
<b>Figure 7:</b>	SCMED with Forced Convection	39
<b>Figure 8:</b>	Variables in the Pipette Flow Calculation	42
<b>Figure 9:</b>	Measured Real Part of Impedance at 3MHz as a Function of Tip to Substrate Distance	46
<b>Figure 10:</b>	The SCMED Apparatus	49
<b>Figure 11:</b>	The Custom Graphical User Interface for Controlling SCMED Fabrication	49
<b>Figure 12:</b>	Nickel Column	51
<b>Figure 13:</b>	Nickel Spring	51
<b>Figure 14:</b>	Surface of the Spring	51

<b>Figure 15:</b> Cross-Section of the Spring Loop Revealing a Hollow Interior	51
<b>Figure 16:</b> Nickel Wall	51
<b>Figure 17:</b> Measurement of the Spring Constant	52
<b>Figure 18:</b> X-ray Diffraction Spectrum	53
<b>Figure 19:</b> Energy Dispersive X-ray Analysis	53
<b>Figure 20:</b> Cell Impedance (Conductivity Measurement)	56
<b>Figure 21:</b> Electrochemical Cell Fabricated for Conductivity Measurements	56
<b>Figure 22:</b> Current Density between Electrodes in the Conductivity Cell	57
<b>Figure 23:</b> Impedance of the KCl Calibration Solution	58
<b>Figure 24:</b> Impedance of the Sulfamate Solution	58

## List of Tables

<b>Table 1:</b> Summary of Micro- and Nano-Fabrication Techniques	15
---	----

## **Chapter 1 : Introduction and Design Philosophy**

A relatively new field is emerging involving the design, construction and use of "micro-electro-mechanical systems" or MEMS. These integrate micro-mechanical components, actuators, sensors, power sources and logic circuits with the goal of building integrated autonomous micro-robots. Potential applications are foreseen in micro-surgery, drug delivery, scientific instrumentation, and the manufacturing of electronic and optical devices [2].

As part of this effort Professor Ian Hunter and his group in the Biorobotics Laboratory are implementing a three staged approach. The first stage involves extending human dexterity and sensation down to the cellular scale and beyond using tele-operated force-reflecting micro-manipulators. The second stage is the development of semi-autonomous, tethered robots, guided and powered through flexible physical links. The final stage is the construction of millimeter and sub-millimeter sized autonomous robots. The latter will essentially be independent artificial life forms, integrating mechanical elements, actuators, sensors, intelligence and power sources. Each stage will complement the next, both in supporting fabrication and by evolving technology and design.

The first stage, namely the building of tele-operated force-reflecting micro-manipulators, is well underway. The combination of parallel actuation and beam bending in the design has allowed the construction of robot limbs capable of multiple degrees of 6 degree of freedom motions, and minute displacements (as little as 1 nm), with high dynamic range of motion ( $>6 \times 10^6$ ), and large displacement bandwidths ( $>1$  kHz). Several manipulators incorporate these features, including two general purpose micro-manipulators (MR-1 and MR-2) [3], a micro-surgical robot with associated virtual environment (MSR-1) [4], and a robot developed in collaboration with MBP Technologies of Montreal, designed to assist

in the fabrication and assembly of micro-systems, such as integrated circuits and MEMS (MFR-1). More recently work has begun on a micro-robot capable of Angstrom scale motions to be used for scanning tunneling microscopy and eventually atomic force microscopy and atomic scale surface modification. Also, a robot (MSR-2) is currently being designed which should allow a surgeon to perform operations such as coronary bypass surgery on a beating heart. (Currently many operations require stoppage of the heart, and thus added complexity and risk.) In an effort to extend the capabilities of these robots, and as part of the progression towards autonomous devices, the incorporation of micro-fabricated end effectors is planned. One manipulator design being considered is a millimeter sized instrumented hand, which is especially suitable for tele-operated systems.

The building of such a device requires a fabrication process able to produce three dimensional structures such as joints and limbs, necessitating (1) a truly three dimensional fabrication capability, (2) sub-micrometer spatial resolution and, ideally, (3) a range of available materials suitable for constructing electro-mechanical devices. Also, (4) the fabrication should occur at reasonable rates such that micrometer to millimeter sized structures can be produced within a matter of hours, or less.

Investigation of current micro-fabrication methods, as presented in Chapter 2, demonstrates that the required fabrication technology does not exist. The fabrication of three dimensional structures such as bearings, pipe networks and closed interstices with sub-micrometer resolution is not possible using current technology, impeding the progress of MEMS development.

Two technological limitations are encountered. (1) The dominant MEMS fabrication technologies are restricted to the production of low aspect ratio (height to width), essentially two dimensional structures. These technologies, including photo-lithography, are inherited from microelectronics, where rapid progress has been made in the miniaturization of circuit elements, and where the formation of two-dimensional, planar arrays is appropriate. (2) The

non-existence of 3D fabrication methods is exacerbated by the lack of 3D assembly technology.

In order to overcome these limitations Professor Hunter invented a three dimensional material deposition process[5]. The process involves localized electrochemical deposition and is known as Spatially Constrained Micro-Electro-Deposition (SCMED). Deposition is localized by constraining the electric field distribution in solution to a small region where forming is desired. Others have also recognized the limitations of current fabrication technology and have begun developing high aspect ratio and truly 3D techniques. Chapter 2 discusses the relative merits of the various approaches.

This thesis describes work I performed over the past 1.5 years to implement three dimensional localized electro-chemical deposition. As alluded to, Chapter 2 reviews current microfabrication technology. In Chapter 3 electro-chemical theory is described as applied to localized electro-deposition. Both the mechanism of localization and factors affecting deposition rates are discussed. Reasons behind the modification of the process from its original implementation, involving forced convection, to its present form employing sharp tips to contain electric field are described in Chapter 4. Finally, Chapter 5 and 6 present the current implementation and the structures grown using it, including a helical spring and a 10 $\mu$ m diameter column. Plans to better understand the process, to improve spatial resolution, to try new materials and to perfect deposition control are outlined in Chapter 7. First, however, a general discussion of micro- and nano-technology completes this chapter, including a description of the most successful MEMS technology to date – Nature's.

## **1.1 Opportunities in Nanotechnology**

In late 1959 the American physicist Richard P. Feynman proposed the fabrication of mechanical and electrical systems on the atomic scale [1]. The benefits, he speculated, might include ultra-high density information storage capable of containing a library's knowledge

on the surface of a library card, micro-robots that course through arteries to repair faulty valves in the heart ( "surgeons you can swallow" ), the direct scanning and modification of DNA, and molecular synthesis atom by atom. Note that when Feynman presented these ideas 4 kbyte core memories filled a small room and IC's were a new invention [6].

Since then others have espoused the "nano-technology revolution" (e.g. Eric Drexler [7]). Transistors have been produced with dimensions of less than 300 nm and sub-millimeter electro-mechanical structures, including <1 mm diameter rotational magnetic micro-motors [8] built. Single atoms can be manipulated in two dimensions using Scanning Tunneling Microscopes [9]. Atomic force microscopes can resolve the helical structure of DNA [10].

The integration of mechanical and electrical components in sub-millimeter sized devices has been chosen as a field of future economic importance. The Japanese Ministry of International Trade and Industry (MITI), in particular, is investing 250 M\$ U.S. over 10 years in the research and development of tele-operated micro-machines including catheters, automated pipe inspectors, and the construction of a millimeter-sized submarine [11]. Total annual Japanese expenditure on MEMS research, including both government and industrial sources, is approximately \$100 M\$ [12]. The Europeans invest approximately the same amount in MEMS, about half the money coming from the government. (In North America, by contrast, governments directly invest only about \$11 M\$ annually [12].)

Silicon MEMS are already being widely used as force and pressure sensors, particularly in the auto industry [12]. Energy conservation regulations in the United States forced auto manufacturers to develop closed loop fuel systems, which measure the oxygen content of exhaust. As part of these systems absolute pressure is measured using Si-based sensors. These are capable of withstanding the tough operating conditions (-40 to 125°C, gasoline atmosphere), with high reliability (over a 10 year lifetime, failure rates of a few parts per million) and at low cost (10 \$ U.S.). 25 million such pressure sensors are produced annually

for the automotive industry. Silicon micro-machined pressure and force sensors are beginning to be used in many products including altimeters, disposable blood pressure transducers for use with intravenous systems, smart suspension systems, air bag accelerometers, and smart munitions.

Benefits of micro- and nano-technology that are commonly cited include[2]:

- (1) Speed. Small systems tend to be relatively fast, due to reduced transit distances and high resonance frequencies.
- (2) Space and Materials. The reduction in size provides savings of space and of materials, both scaling with the third power of dimensions.
- (3) Workspace and Access. Clearly, miniaturized systems can enter environments that cannot be reached by larger entities. This aspect is relevant in microsurgery, for example, where access to arteries, the eye, sections of the brain etc. is desired.
- (4) Upwards Engineering. Large scale structures can be built with micrometer or eventually nanometer detail, as nature has so successfully done.

The future of nanotechnology is linked to the development of enabling technology and, in particular, of fabrication technology. Fabrication is key because all aspects of MEMS, including mechanical elements, circuits, sensors, actuators and power sources must be built and integrated. Thus the shape and substance of MEMS are constrained by the capabilities of fabrication methods.

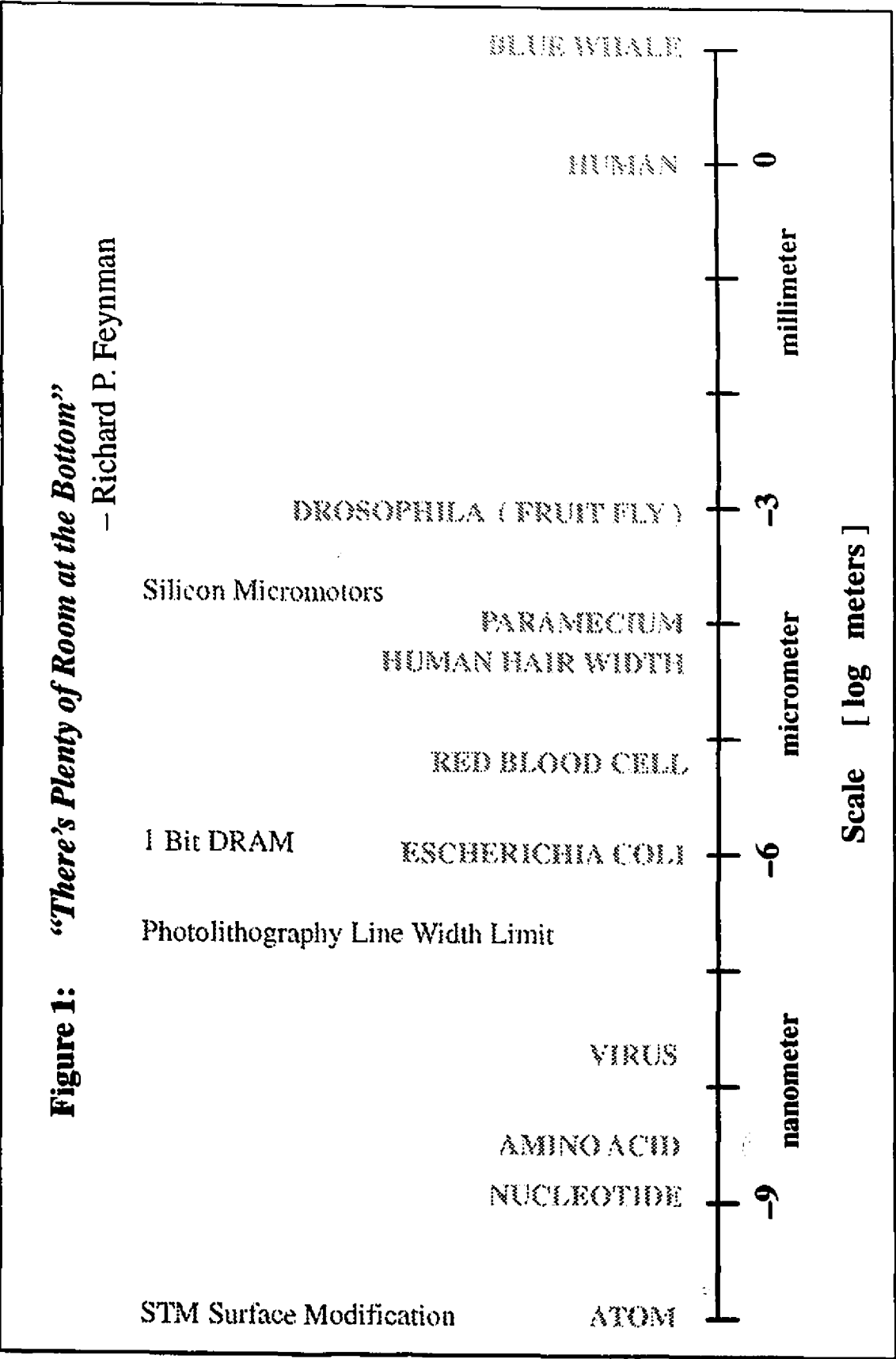
Feynman recognized that nano-fabrication is essentially an engineering challenge, the fundamental physics being understood well below the atomic scale[1]. Nature has proven that molecular level fabrication is indeed physically possible and has applied it to produce organisms ranging in size from several nanometers up to tens of meters. The next section briefly describes nature's fabrication accomplishments and methods.

## 1.2 Nature – A View into the Future?

Feynman proposed several applications of nanotechnology, many of which, it turns out, were present within him as he spoke! In DNA, for example, as Feynman recognized, one bit of information is encoded by about 25 atoms, occupying a volume of  $0.5\text{nm}^3/\text{bit}$ . At such a density, the text contained in all the world's books ( $\sim 10^{15}$  bits [1]) could be stored in a ball of material approximately a tenth of a millimeter in diameter. Repair enzymes routinely scan DNA for mutations. Surgical submarines are in the form of macrophages activated by T-cells to gobble up invading pathogens. All this is made possible by nature's molecular fabrication system.

Evolution has been an “upward engineering” process, building from molecular origins to span 10 orders of magnitude, as outlined in Figure 1. Organisms remain dependent on molecular scale interactions. The information required for growth and survival is encoded in DNA molecules, and each live cell in an organism contains identical replicas [13]. DNA has a double helix structure, the helix being 2 nm in diameter and each loop is 3.4 nm long. Information is encoded in four bases (Thymine, Cytosine, Adenine and Guanine), and there are 10 base pairs per loop. Enzymes unravel the double helix to read and copy the sequence of bases (transcription) at a rate of about 500 base pairs per second in procaryotes (e.g. *Escherichia coli*) and, due to packaging, at about 50 base pairs per second in eucaryotic cells (e.g. human) [14]. The copy (RNA) is transported to the site of translation (ribosome), where protein synthesis occurs, one amino acid at a time. Three bases form a “word” or codon corresponding to one of 20 amino acids, the sequence of codons describing the structure of the protein. Translation occurs at a rate of approximately 15 amino acids per second, and thus an average protein (300–500 amino acids long) is produced in 25–30 seconds [14]. (e.g. Actin micro-filaments, which are involved in movement within a cell and of a cell as a whole, polymerize spontaneously from proteins approximately 180 amino acids in length, corresponding to about 540 codons of information. Myosin, which acts on actin to produce

**Figure 1:** *“There’s Plenty of Room at the Bottom”*  
 – Richard P. Feynman



muscle contraction, is composed of single chains 1,800 amino acids long, the longest single polypeptide chains yet observed in nature [15].) The portion of DNA describing one protein generally corresponds to a gene, the unit of genetic inheritance. Three billion base pairs form the human genome, allowing the storage of up to  $10^{10}$  bits, while *Escherichia coli* bacteria contain 4 million base pairs and simple viruses about 5 thousand.

The molecular basis of life allows a wide variety of materials, organic and inorganic, to be formed, dismantled, repaired and regenerated. Cells differentiate and divide to form tissues, neurons grow connections and bone is deposited in a composite matrix of inorganic materials (calcium carbonate and calcium phosphate) and collagen fibers. In bone formation, cells (osteoblast and osteoclast) are hormonally directed to lay down or remove the organic matrix into which the calcium complexes are deposited. These activities are all governed by molecular feedback pathways and information encoded in DNA.

The molecular basis has also enabled the construction of electro-chemo-mechanical systems whose sizes range over 10 orders of magnitude. These are composed of “custom” organic molecules, polymers and composite materials, and integrate molecular-based actuators (e.g. muscle), complex three dimensional, and highly parallel computer architectures ( $\approx 10$  billion nerve cells making  $10^{13}$  interconnections) as well as chemical (taste, smell), electro-mechanical (hearing, touch) and electro-optical (vision) sensors.

### **1.3 Biotechnology and Fabrication**

If nature is so good at building MEMS, why not exploit its fabrication mechanisms? Viruses, after all, which are unable to reproduce themselves, use this approach. They inject their string of DNA or RNA into a cell, which very generously replicates the nucleotides until the host explodes. One might use nature’s molecular fabrication methods to customize single cells, then move to produce tissues and perhaps even onto the growth multi-cellular organisms.

Researchers routinely use viruses to add and delete genetic material in a technique known as viral splicing [13]. Viruses can, for example, incorporate genetic material at random locations in the DNA, allowing researchers to add a particular trait to a cell. Micro-patterned surfaces, fabricated using microelectronics technology, are used to direct neuron growth [16][17], and ultimately to form live neural networks [18].

However, although some of the fabrication mechanisms such as the forming of proteins and bone and the mechanisms involved in cell division are gradually being understood they are enormously complex. Gene expression, for example, is often determined by elaborate feedback pathways. Artificial DNA synthesis can be achieved but only in lengths of a few hundred base pairs, while a single gene can contain up to 2 million such pairs. Apart from the complexity of biological systems, and thus the time it will take to develop biologically-based artificial organisms, there are several other reasons why an alternate approach is advantageous. Biological systems can only survive in a limited range of environments. If temperature is raised much above 60°C, proteins denature (i.e. lose high order structure such as a helical shape or a globular conformation determined by hydrogen bonds, and thereby lose normal biological activity). Below freezing, life, which is water based, stops temporarily at least. Absence of oxygen or CO<sub>2</sub> is generally fatal since these are crucial for energy production, while exposure to radiation destroys organic molecules. The sensory range is limited; Nervous system transmission is extremely slow compared to those of electromagnetic devices ( 100m/s versus  $3 \times 10^8$  m/s ); A large and complex infrastructure is required in most "big" organisms, including the circulatory, respiratory and excretory systems, and so on. While it may be that some of these limitations could be overcome using human ingenuity, that same ingenuity can also be employed to discover new approaches to fabrication, complementing and exceeding the capabilities of biologically-based systems.

## 1.4 Effects of Scaling

It is interesting to observe that nature often takes rather different approaches to building structures than we do. This may largely be due to the combination of scaling considerations and life's molecular origins. As dimensions are reduced the surface area to volume ratio increases. Thus surface forces (e.g. chemical, electrostatic and viscous) become increasingly significant relative to body forces (inertia, gravity). Life apparently began on the molecular scale, a regime where surface forces are clearly dominant over body forces, and, despite evolution to the macroscopic scale, it has maintained a dependence on molecular mechanisms. Human built structures, on the other hand, have, until recently, generally involved parts and processes acting on scales of greater than a millimeter, where body forces are generally dominant.

Conventional actuators such as combustion engines, electric motors and inertial propulsion mechanisms become increasingly ineffective as their dimensions are reduced [2]. In inertial propulsion systems, for example, Reynold's number tends to zero as dimensions are reduced, rendering them useless, while combustion engines lose heat too rapidly to generate much pressure [1].

Given the molecular origins of biological systems, it follows that surface forces were dominant early on in evolution. The molecular dependence has been maintained. Biological actuators such as muscle, for example, employ molecular contractions to generate force and motion. Muscle consists of myriads of myosin heads ( $10^{23}$  heads/m<sup>3</sup>), which ratchet along in 50 nm steps at rates of several hertz [14]. Bacteria encounter relatively large viscous forces (low Reynold's number) so flagellates propel themselves using a spiral motion, like that of a corkscrew, rather than by accelerating fluid, as is done by propellers, jets and rockets.

Reduction in size also affects mechanical properties. Griffith [19] demonstrated in 1920 that as fiber diameters are reduced below about 500  $\mu\text{m}$ , tensile strengths rise well beyond

the bulk value. This effect is attributed to a reduction in surface defects which result in fracture and failure.

MEMS researchers are thus investigating many new actuator technologies, including magneto-strictive materials, shape memory alloys, contractile polymers [20] and electrostatic actuators<sup>1</sup>. In Professor Hunter's group, for example, efforts are focussing on the development of contractile nickel titanium fibers [22] and contractile polymer actuators .

### **1.5 Downward Engineering – From Macro to Micro.**

Feynman proposed a sequence of scaling operations by which a “master-slave system” with a miniaturized slave is used to build a yet smaller version of itself, which in turn is connected to the master, and used to construct another yet smaller version and so on in a geometric series. No one as yet has successfully implemented such an elegant approach. Instead, miniature devices are being fabricated directly using macroscopic tools.

The microelectronics revolution has evolved many highly developed methods [23] which have steadily brought resolution down to micrometer and sub-micrometer scales. Thin films, ranging in thickness from a single atomic layer up to a few micrometers, are grown by various means. Photo-lithography then images macroscopic 2D patterns, corresponding to circuit elements and interconnections, onto these layers, chemically altering them to allow the incorporation of lateral features.

Photo-lithography produces thin, flat structures which are well suited to microelectronics applications, for which the process was designed, but which are far from ideal if mechanical components are to be integrated. Nevertheless, the lack of real alternatives has made photo-lithography the most widely used MEMS fabrication technology. At the 1994 IEEE Micro Electro Mechanical Systems conference [24], for example, 65% of the presentations involved fabrication using photo-lithography to construct silicon or gallium arsenide based

1. See Hunter and Lafontaine [21] for a comparison of the various actuator technologies with the properties of muscle.

structures. Of the remainder, most used microelectronics related technology such as ion-beam milling through a mask or simply involved thin films deposition. Only 5% of the total employed truly 3D techniques. While interesting structures have been built using silicon-based technology (including spinning micro-motors with sub-millimeter rotor diameters [25][26]) successful applications have so far been few. Exceptions are silicon beam force transducers, pressure sensors, and strain gauges, applications in which low aspect ratio is not a disadvantage [12]. The major limitations of micro-electronics-based technology are the narrow range of available materials (i.e. largely silicon and gallium arsenide based) and the low aspect ratios produced [27].

In the next chapter, a description and an evaluation of current micro- and nano-fabrication technologies are given.

## Chapter 2

# Overview of Micro–Fabrication Technology

In this Chapter micro–fabrication technologies are described, with the aim of determining their current capabilities and future prospects. Before reviewing the state of the art in micro– and nano–fabrication, some general concepts are discussed which are used to classify the utility of the various techniques.

There are two basic classes of fabrication methods: those involving material removal and those that add or shape material. Examples of material removal processes are carving, laser cutting and milling. Material addition and shaping processes include moulding, painting and electrodeposition.

### 2.1 Material Removal

Material removal methods have two fundamental limitations. Firstly they are limited to the properties of the material that they are cutting. If variations in the conductivity or the modulus of elasticity, for example, are desired in the object being constructed then either an appropriate chunk of matter must be selected or interlocking parts must be separately built and assembled. Secondly, material removal methods are restricted in the geometries they can achieve. Closed interstices and helices for example are difficult or impossible to fabricate.

Despite these limitations material removal methods are ubiquitous in manufacturing. Both drawbacks can be overcome using assembly techniques, at the expense of time and complexity, but nevertheless often proving advantageous given the alternatives. On the micrometer and nanometer scales however, assembly technology is very primitive and for many operations does not exist. Microelectronics technology allows the bonding of wafers and the attachment of small wires (<100  $\mu\text{m}$  diameter) but the manipulation of objects is dif-

difficult as they reach dimensions of  $\leq 40 \mu\text{m}$ . Therefore the use of material removal methods alone to produce moderately complex micro-structures such as a miniature hand is not currently feasible.

## 2.2 Material Addition

Material addition can be done in parallel or in series. Moulding, electroplating and epitaxial growth are examples of parallel deposition, while painters, inkjet printers, and cake decorators perform deposition serially.

Moulding procedures require the construction of a negative and are thus limited by the technique used to construct the mould. Furthermore, the complexity of the object is restricted by surface tension and adhesion problems and by the difficulty of using more than one material. Nearly closed interstices are possible, providing that the negative can somehow be removed. Like moulding, electroplating and epitaxial growth are parallel fabrication methods. These create laterally homogeneous layers.

In principle serial deposition procedures allow the greatest freedom in terms of both geometry and material variations ( providing of course that a range of materials is possible with the given procedure and that these are compatible ). In two dimensions, for example, the use of a fine tipped brush allows the incorporation of a level of detail and a variety of colours not possible with a roller. If the roller and the brush can be moved at the same speed, however, the roller can fill a space much more rapidly. The relative speed disadvantage of a serial process can be overcome by having many serial elements working in parallel and/or very rapid individual serial elements.

Thus in principle serial deposition techniques allow the greatest flexibility in geometry and material properties. These features are essential in constructing moderately complex structures on micrometer and nanometer scales due to the lack of effective means of assem-

bly. They are also intrinsically more efficient because assembly steps and material waste are minimized.

## 2.3 Fabrication Techniques

Apart from geometry and material variability, fabrication processes are also judged on the bases of spatial resolution (i.e. the smallest cut or deposit possible), fabrication rate, and the variety of workable materials available, among other criteria. Table 1 summarizes the strengths and weaknesses of the various methods discussed here. The numbers represent current capabilities unless accompanied by a question mark. Note that resolution, rate and the materials used are not always independent of each other. Rates listed are peak values found in the literature for sub-millimeter resolution fabrication, while resolutions are simply the highest found. The dimensions column indicates the achievable geometry. 2+ denotes a high aspect ratio capability with little or no vertical resolution (2D with thickness), while 3- indicates that while 3D geometries are achievable, many configurations are not possible (e.g. closed interstices). Figure 2 at the end of the chapter summarizes the table data by plotting rate versus resolution for 3D fabrication methods.

**Table 1: Summary of Micro- and Nano-Fabrication Techniques**

	Dim.	Resolution [nm]	Materials	Rate [nm/s]	+’s and -’s
Photo-lithography	2	250 e.beam: 10	mainly Si based, GaAs	-	+ Parallel - Low aspect ratio.
LIGA related	2+	1 000 features	PMMA Ni, Au +	-	+ Aspect ratio - Geometry.
<b>MATERIAL REMOVAL</b>					
Excimer Laser	3-	200	Polymers, Met- als, Ceramics.	2500 (polyimide)	+ Materials. - Geometry, Aspect
Electron Beam	3-	2	Various Crystals	25	+ High Resolution - Low Rate
Ion Beam	3-	1 ⊥ 100	Various.	10	+ Surface Finish. - Low Rate
EDM	3-	2 000	Conductors	500 000	+ Rate - Resolution
<b>MATERIAL ADDITION</b>					
Stereo Lithography	3	5 000	UV Polymer	2000	+ Geometry - Materials - Resolution
Powder Deposition	3	10 000	Ceramics, Composites	1 000	+ 3D - Resolution
LCVD	3	10 000 e.beam: 200	B, W, Si	1000 e.b.20	+ Geometry - Resolution
STM	2	0.2	atoms	0.1	+ Resolution - Rate
<b>ELECTROCHEMICAL METHODS</b>					
Electroless Plating	2+	1 000	Plating Metals	40	+ Forms on Non- conductors - 2D
LEEP	2	2 000	Electrodeposits	6000	+ Rate - 2D & Resolution
SECM	2	300	Metals Polymers	-	+ Resolution - 2D
Localized Electro- Deposition	3	< 10 000 <300 ?	Metals Alloys? Polymers?	> 6000	+ Rate, Resolution + Materials - Serial

## **2.3.1 Conventional Fabrication**

Conventional fabrication techniques, such as milling, can produce mirror finishes, but are hard pressed to build  $< 100\mu\text{m}$  features. In machining processes tool size, tool wear and the stresses involved make smaller features difficult to achieve.

## **2.3.2 Photo-Lithography and Related Methods**

### **2.3.2.1 Photo-Lithography**

Photo-lithography is a standard technique developed for and used in printed circuit fabrication [23]. In a standard configuration a thin film of material such as polysilicon is grown on a substrate followed by a layer of protective resist. The resist is irradiated through a mask, creating an exposed pattern whose susceptibility to etching is altered. Etching then transfers the pattern to the underlying thin film. Note that photo-lithography combines parallel material deposition and removal.

Lateral feature size is ultimately diffraction limited and thus the finest features are on the order of 200 nm when visible light is used. However, the use of electron [28][29] and x-ray [30][31] beams has brought resolution down to tens of nanometers. Undercutting of the etchant beneath the mask limits both lateral resolution and depth, while photon absorption by the resist also limits depth. Thus aspect ratios (height to width) seldom exceed 0.5 when conventional wet etching is used [32], constraining photo-lithography's utility for constructing three dimensional structures. Anisotropic etching techniques have been developed, in which material is preferentially removed in one direction, allowing aspect ratios of up to 100 to be achieved. However, such aspect ratios are achieved at the expense of features in the etched direction. In other words, they result in relatively thick slabs of material with a two dimensional pattern etched through the the thickness.

To improve aspect ratio and add complexity multiple layers have been deposited. Unfortunately these can be difficult to align so that few structures contain more than three or four.

Nevertheless some impressive structures have been built using multi-layering such as silicon disk micro-motors [26][33] and  $2\mu\text{m} \times 2.5\mu\text{m}$  square polysilicon tubes [34]. Given the current restrictions on the number of layers, there is a tradeoff between layer thickness and thus aspect ratio, and feature size in the third dimension.

The main disadvantages of photo-lithography are that (1) it is often restricted to planar, low aspect ratio structures by etching undercut, the penetration depth of photons into the resist materials, and the lack of 3D assembly techniques. Anisotropic etching allows high aspect ratios to be achieved at the expense of resolution in the third dimension; (2) Even moderately complex structures require multiple layering, which increases production time and decreases yield; (3) Finally, it is Si and GaAs based whereas for many applications metals, polymers and ceramics would be more suitable.

### **2.3.2.2 LIGA and High Aspect Ratio Lithography**

Several techniques have been developed which bring high aspect ratio to photo-lithography [32][35][36]. Resist materials are used which are deeply penetrable by electromagnetic waves. Thick resist layers are deposited, followed by exposure and etching, as in photo-lithography. However, only the resist is etched, and it is preserved as is or employed as a mould.

The first and perhaps the best known of these high aspect ratio processes is known as LIGA [35][37], an acronym derived from the German for lithography, plating (galvanometric) and moulding (abformung). In LIGA, high energy synchrotron x-rays pass through a mask to irradiate an x-ray sensitive polymer. The polymer is etched to provide a mould, which is filled with electroformed nickel or gold. The highly parallel and penetrating x-rays allow layer thicknesses of  $>300\mu\text{m}$  [38], with sub-micrometer accuracy.

LIGA has been used to build micro-motors with  $300\mu\text{m}$  thick nickel rotors, providing much improved inertia compared with the micrometer thick polysilicon versions [27]. Gears

and layered structures have also been fabricated, having lateral features down to  $\approx 2 \mu\text{m}$  [39].

Many laboratories do not have access to synchrotron beams, but there is an alternative. Ultra Violet light can be used to expose photosensitive polyimides, enabling the patterning and etching of sharp side walls with depths of up to  $\approx 85 \mu\text{m}$  and lateral features several micrometers across [32].

The high aspect ratio of LIGA and related techniques is produced at the expense of vertical resolution. The two dimensional mask pattern on which the structures are based does not allow for variations in the third dimension, except by the incorporation of a sequence of layers. However, each layer is of uniform thickness and thus again there is a tradeoff between layer thickness, vertical resolution, and fabrication time. As with photo-lithography, LIGA-based methods are restricted by the lack of assembly tools and the complexity of producing multi-layered structures. Even simple structures such as helical springs and closed interstices are difficult if not impossible to produce.

### **2.3.3 Material Removal Methods**

In this section microfabrication techniques involving material removal are considered, including photon and electron beam methods, and electrical discharge machining.

#### **2.3.3.1 Excimer Laser Ablation**

Excimer laser wavelengths are highly absorbed by most materials [40]. The three standard excimer lasers are krypton fluoride (248 nm wavelength), xenon chloride (308 nm) and argon fluoride (193 nm). Photon energies are sufficient to break co-valent bonds, the bond destruction being accompanied by the ejection of the freed molecules due to local volume changes (ablation). Because photon energies are sufficiently high to interact directly with bonds, short pulses (nano-seconds) are generally employed to remove material, avoiding unnecessary heating and thus thermal damage of regions surrounding a cut. Infra-red lasers,

on the other hand, use lower energy photons which produce local heating. Material is melted and then evaporated, resulting in thermally induced damage to the surrounding region [41]. Not only does the shorter excimer laser wavelength allow cleaner cuts, but it also results in reduced diffraction and thus higher resolution. For these reasons excimer lasers are preferred over infra-red lasers in microfabrication and in some surgical procedures, such as corneal machining.

Excimer machining may be done in series, using focussed beams [42], or in parallel, by imaging a mask onto a surface [43]. Sub-micrometer features are possible and many materials are used including ceramics [41], polymers [43] and metals [42]. Diffraction limits feature size to the order of a wavelength. Also, high resolution is produced at the expense of depth since numerical aperture must be increased and depth of focus reduced in order to decrease focal spot size.

### **2.3.3.2 Ion Milling**

In the ion milling process a stream of ions bombards a surface, physically dislodging the atoms [44]. Inert species such as Argon ions are normally used to avoid chemical reaction of the ions with the surface material. Ion beams are either focussed or projected through a mask. Atomic resolution is possible parallel to the machined surface, and the normal resolution is about 100 nm for reasonable bombardment rates. Typical milling rates are still only on the order of tens of nanometers per second however [45][46]. Furthermore secondary effects including ion reflection and the redeposition of ejected material make it difficult to produce high aspect ratio structures using this technique.

In etching procedures such as Reactive Ion Etching (RIE), ion milling is combined with more rapid but isotropic chemical etching to produce rapid, materially selective and anisotropic removal. RIE and related processes are often used to increase aspect ratio in photolithography [47].

### **2.3.3.3 Electron Beam Milling**

High energy electron beams can be highly focussed given their short wavelengths (a property which is taken advantage of in electron microscopy). A group at Cambridge University has milled holes  $2.0 \pm 0.2$  nm in diameter and  $>200$  nm deep using such beams in several materials including alumina, NaCl, CaF<sub>2</sub>, MgO and AlF<sub>3</sub> [48]. Incident electrons ionize atoms resulting in surface desorption. Unfortunately milling rates are too slow (25 nm/s) for application on larger scales.

In a recent development, the same Cambridge group has discovered that the application of an electron beam to SiO<sub>2</sub> can reduce it to silicon, allowing the production of 2 nm diameter silicon wires [49].

### **2.3.3.4 Electrical Discharge Machining**

Electrical discharge machining or EDM is used to machine conductors [50]. Sparking is induced between a tool piece and the worked object causing localized heating and material removal. A low voltage high amperage current is switched on and off at up to 200 kHz to produce the sparking. The tool to material separation is servo-controlled using current feedback to control sparking and adjust feed rate. Discharge normally takes place through a flowing liquid dielectric which carries expelled material away. EDM is used in industry to machine very hard conductors such as carbides for which inertial cutting is difficult.

In EDM the tool has a tendency to wear rapidly as it is itself eroded by the electrical discharge. The erosion is particularly significant on the micrometer scale. A variation on EDM called WEDM (Wire EDM) avoids wear by using a continuously replenished wire as the cutting tool. WEDM resolution is thus limited by wire size (e.g. 20  $\mu$ m for the Charmilles Special, Charmilles Technologies, Switzerland), while the wire shape restricts accessible geometries. Although not widely used in constructing micro-electro-mechanical systems, it is useful for the construction of cylindrically symmetric objects such as rods and nozzles [51].

## **2.3.4 Material Addition Methods**

Several methods capable of producing three dimensional structures are described, including UV lithography, Laser Assisted Chemical Vapour Deposition, and Powder Deposition.

### **2.3.4.1 Stereo Lithography**

In stereo lithography truly three dimensional structures are formed by making use of the interaction between a focussed light beam and a photo-sensitive polymer. When the beam is focussed into the polymer it is locally hardened. The focal point trajectory is used to form objects. Industry employs the process for rapid prototyping. It is not generally used to form working prototypes, however, because of the polymer fragility. Structures can be used as moulds, though this process requires the application of heat resistant coatings, which are slow to apply (days), and which can often be used only once, again due to fragility.

The process has been applied on on the micrometer scale, the impulse response due to the application of the beam at a single point being approximately  $5 \times 5 \times 3 \mu\text{m}^3$  [52] to date. An impressive array of structures have been formed including helices, bent pipes, check valves [52], a simple electrostatic actuator using a conductive version of the polymer, and a system of pipes, pumps and valves eventually intended for use as an Integrated Liquid Chromatography system [53].

Although the application of stereo lithography to the construction of micro-mechanical systems is relatively new, the variety and complexity of structures produced clearly demonstrate the benefits of a truly three dimensional forming process. The drawbacks of the technique are the current unavailability of a wider range of materials and the relatively large minimum feature size achieved thus far. Resolution is ultimately diffraction limited. A further resolution limiting mechanism is destruction of the solidified polymer due to viscous forces from the liquid, which increases as resolution is increased.

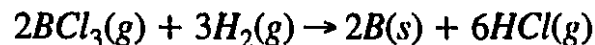
### 2.3.4.2 Powder Deposition

Powder deposition is in direct competition with Stereo Lithography in the rapid prototyping market [54]. Ceramic moulds are produced by repeatedly spreading layers of ceramic powder, each layer being selectively bonded using ink-jet writing of colloidal silica droplets.

Although it produces effective moulds it is not yet a viable micro-fabrication technology due to its large lateral resolution ( $\sim 100 \mu\text{m}$ ). Rapid droplet drying and difficulties in uniformly spreading very fine powders ( $< 5 \mu\text{m}$ ) are hampering efforts to reduce feature size. A related process is under development in which localized electroless plating binds particles. The plating is localized by focussing a laser beam on the particles to be joined, resulting in local heating and greatly enhanced deposition rates. The enhancement mechanism is described in Section 2.3.6.2. Resolution on the order of  $10 \mu\text{m}$  has been achieved in two-dimensions. Results are as yet unpublished.

### 2.3.4.3 Laser Assisted Chemical Vapour Deposition ( LCVD )

In chemical vapour deposition (CVD) a chemical reaction occurs on a heated substrate resulting in the deposition of a solid from the vapour phase. Boron for example is commonly deposited in the reaction:



In LCVD a laser beam heats a localized region of the substrate, effectively localizing the reaction [55][56]. The laser beam focal point is moved in three dimensions to create structures. Structures built include a 2 mm high,  $200 \mu\text{m}$  wide helical boron spring and a tungsten solenoid wound about a silicon rod [57]. Formation rates are on the order of  $1 \mu\text{m/s}$ .

Using visible light sources it is unlikely that LCVD will be capable of sub-micrometer spatial resolution given the combination of diffraction limits and the enlarging effects of thermal conductivity.  $10 \mu\text{m}$  laser spot sizes produce  $15\text{--}20 \mu\text{m}$  diameter boron rods, the enlargement likely due to thermal conductivity [55].

LCVD has been tried with shorter wavelengths. A 248 nm KrF excimer laser was used by Maeda, Minami and Esashi [58] to grow 50  $\mu\text{m}$  wide Chromium lines on a polyurethane tube in building a catheter. The Chromium was found have low conductivity due to carbon contamination, and so far high resolution deposits have not been reported using an excimer laser. Electron beams, however, have been employed to deposit high aspect ratio (6:1), 200 nm diameter tungsten/carbon columns (EBCVD) [59]. Unfortunately growth rates are slow (20 nm/s).

### **2.3.5 Scanning Tunneling Microscopy (STM)**

Scanning tunneling microscopes are capable of providing atomic resolution surface maps of solid conductors [60][61]. Conducting wires with ultra-sharp tips, ending in single atoms, are used as probes. These tips are brought up to a surface. The tip atom's wavefunction overlaps with those of surface atoms, the overlap and thus the probability of electron transfer increasing as the tip to surface distance decreases. If a potential is applied between the tip and the surface, current rises exponentially as the tip to surface separation decreases. By scanning the tip over the surface and using current feedback to remain a constant distance above it, the wavefunctions of the surface atoms can be mapped.

STM tips have also been used for surface modification. Methods include scratching nanometer wide lines, depositing material from the tip onto the surface [62], inducement of electrochemical reactions [63], etching or deposition by field evaporation (in effect a nano-electrical discharge machining) [64] and the actual manipulation of individual atoms to form patterns[65]. Perhaps the best known atom manipulation was done by researchers at IBM who managed to drag individual Xenon atoms across a surface to write the letters I B M [66].

While atomic resolution is well beyond that needed to fabricate the micro-manipulators and microsurgical robots envisaged here, and the forming rates are too slow for construction

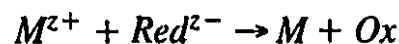
of the much larger structures, the artificial organisms of the future may well be fabricated atom by atom using an STM-like process.

## 2.3.6 Electrochemical Methods

In conventional electroplating thin films of material are deposited indiscriminately over a surface. The building of mechanical structures and circuit elements requires greater selectivity. In microelectronics, photo-lithography can be used to etch the desired patterns in an electrodeposited layer. Several other means of selective deposition also exist. Although these are generally restricted to the construction of two dimensional patterns or to electro-forming (filling moulds), the concepts involved are relevant to the discussion of the three dimensional localized electro-chemical deposition process. Thus electroless plating, Laser Enhanced Electro-Plating and Scanning Electro-Chemical Microscopy are all discussed as an introduction to the ideas behind Spatially Constrained Micro-Electro-Chemical Deposition (SCMED).

### 2.3.6.1 Electroless Plating

Electroless plating is often used in the microelectronics industry to fill via holes because no potentials need be applied to drive the reaction and thus conducting substrates are not required [23]. Instead a reducing agent provides the chemical potential necessary to induce deposition. A typical reaction for the reduction of a metal,  $M$ , for example might be:



In order for this reaction to proceed the surface must be catalytic. Thus by selectively varying surface materials the deposit can be localized. For example, silicon is catalytic to nickel plating while  $SiO_2$  is not. Photo-lithography can thus be used to mask a Si surface with  $SiO_2$  [67].

When high aspect ratio structures are desired, electroless plating can be used to fill moulds, a process known as electro-forming. Via holes [68] and LIGA structures [35] are

examples of structures built by electroforming. Deposition rates for electroless forming are on the order of 100  $\mu\text{m/hr}$  [23].

### **2.3.6.2 Laser Enhanced Electro-Plating (LEEP)**

Conventional electroplating and forming rates are diffusion limited. Electron transfer to the depositing ions occurs much more rapidly than ions can be transported to the surface, creating concentration gradients. Diffusion becomes the primary transport mechanism in this depleted region, and thus is rate determining, constraining deposition rates to approximately 100  $\mu\text{m/hr}$  [69].

Von Gutfeld and his colleagues at IBM found that rates of deposition can be enhanced by three to four orders of magnitude by shining a laser beam onto a surface [70][71]. The rapid localized deposition is apparently due to local heating which (a) increases charge transfer kinetics, (b) shifts the equilibrium potential and (c) induces micro-stirring. The micro-currents, driven by temperature gradients, result in the influx of undepleted solution to the surface. If sufficient laser power is used local boiling occurs, further increasing mixing and thus deposition rate.

LEEP has been used to deposit copper and gold lines with widths  $\geq 2 \mu\text{m}$ , at forming rates on the order of 20  $\mu\text{m}^3/\text{s}$ , corresponding to a vertical deposition rate of  $\approx 6 \mu\text{m/s}$  [70][71]. Such deposition rates make a localized electrochemical process for fabricating 3D structures feasible. Unfortunately as the depth of the deposit increases, so does the lateral thermal conductivity, dissipating the thermal energy and enlarging features. The combination of thermal degradation of resolution and the diffraction limitation of the visible wavelength laser used make it unlikely that LEEP will be able to produce three dimensional structures with sub-micrometer resolution in its current configuration. It has however found an application in making and repairing circuit board connections [72].

The concepts involved in understanding Laser Enhanced Electro-Plating are also important to SCMED, and are discussed in some detail in Chapter 3.

### 2.3.6.3 Scanning Electrochemical Microscopy

Scanning Electrochemical Microscopy (SECM) is a variation of STM for the study of the chemistry and surface structure at solid–liquid interfaces [73]. The probe electrodes are generally identical to those employed in STM, except that they are coated up to the tip to reduce Faradaic currents. Unlike STM, where the probe electrodes are in relatively inert surroundings, such as air, nitrogen or vacuum, the surrounding solution in an SECM study is liquid and often conductive, and thus the insulating coating eliminates all currents except those emanating from the electrode tip. Coated tips allow tunneling current to be resolved and thus surfaces to be mapped [74]. At large tip to substrate distances, where tunneling current is no longer observed, feedback on the faradaic current is possible [75]. Furthermore these ultra–micro–electrodes are excellent for performing local electrochemical measurements such as voltammetry [76].

Coated tips have also been used to etch and deposit material. The sharp tips used in STM and SECM concentrate field lines such that when they are in close proximity to a surface, the field is localized. Since electrical potential drives the deposition (or etching) of ions, the deposit (or material removal) is also localized. Lin, Fan and Bard were the first to achieve localized etching [77]. They were able to electrochemically etch a 300nm wide line on a GaAs substrate. Schneir et. al. subsequently demonstrated the electrodeposition and STM imaging of a 300 nm wide, 1.2 $\mu$ m long and >100 nm high gold line on a gold surface [78]. The deposition and imaging were done using the same tip.

Bard and his colleagues have since deposited silver [79], copper, palladium [80][81] and polyaniline [82] lines. The metal lines all had widths of  $\approx 0.5 \mu$ m while the polyaniline deposit was 2  $\mu$ m wide. However, this deposition was not done in aqueous solution, but rather through thin ( $\approx 100 \mu$ m) ionically conducting polymer films. They chose the polymer films over aqueous solutions for three reasons [80][81]:

(1) In order to localize field effectively, and hence the deposit, the electrode must be positioned within approximately a tip diameter of the substrate. Faradaic current is only sensitive to tip-substrate distance within approximately one tip diameter [83], making position control difficult. When the polymer film is used the electrode is not coated. The faradaic current varies in proportion to the square root of the tip area immersed in the film, reportedly providing better feedback.

(2) In aqueous solution deposition onto, or etching of the tip apparently occurs, resulting in either tip enlargement and thus a degradation in resolution, or tip passivation, and thus no deposition. The electrode appeared unaffected in the solid electrolyte.

(3) Finally, the fabrication of coated electrodes with exposed areas of less than  $1\mu\text{m}^2$  is difficult, whereas the tips used with polymer films require no insulation.

Unfortunately the use of thin films rules out 3D fabrication because electrode motion and thus deposition is restricted to 2D. The concept of SCMED depends on the freedom to move in 3D allowed in aqueous solution. The next chapter describes the principle of SCMED, and how the obstacles have been dealt with.

### **2.3.7 Summary**

Table 1 summarizes the properties of the various fabrication processes described. Figure 2 is a plot of rate versus resolution for the 3D material deposition and removal processes discussed. Note that excimer laser machining is the only process which meets both the rate and resolution criteria. There are two drawbacks to excimer laser machining however (Section 2.3.3.1); High resolution is produced at the expense of aspect ratio, and excimer machining is a material removal method, and is thus restricted in the geometries it can produce. Thus, none of the processes meet the criteria of (1) truly 3D fabrication with (2) sub-micrometer resolution, using (3) desirable materials at (4) reasonable rates.

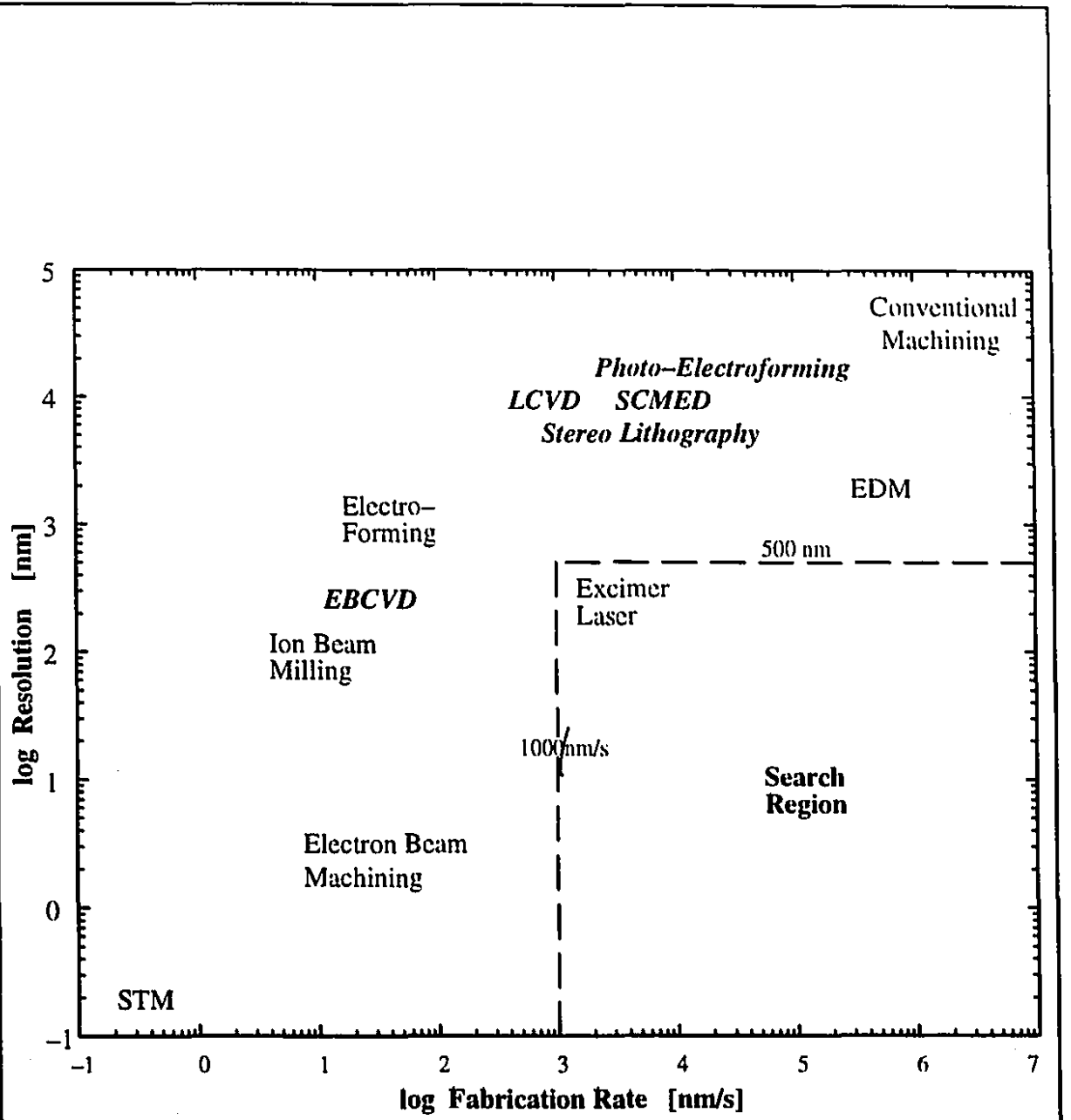


**Figure 2 : Fabrication Rate and Resolution of 3D Fabrication Technologies.**

***Bold Italics*** represent true 3D material addition methods.

The electrochemical methods discussed demonstrate appropriate resolutions (300 nm), materials (metals, polymers) and rates ( $\mu\text{m/s}$ ), but are restricted to 2D. The remaining Chapters discuss the development of spatially constrained electrochemical deposition (SCMED), a 3D electrochemical process which promises to achieve the four fabrication criteria.

## Chapter 3 : Electrochemical Theory

### 3.1 Concept of SCMED

In Spatially Constrained Micro-Electrochemical Deposition (SCMED) [84] the tip of a sharp pointed electrode is placed in a plating solution and brought near the surface where deposition is to occur (Figure 3). A potential difference is applied between the tip and the substrate. Electric field and thus deposition are confined to the region beneath the tip, as demonstrated in Figure 3(a). The tip is then moved with respect to the forming surface to create structures, Figure 3(b). In principle the size of the electrode determines the spatial resolution, and any structure geometry is possible providing it is electrically continuous with the substrate. The electrochemical nature not only allows deposition but also etching and polishing.

Deposition rate and deposition profile are critical to the success of SCMED. This chapter discusses electrochemical theory as applied to deposition rate and profile from micro- and ultra-microelectrodes. Various phenomena affect the deposition of ions from solution onto a substrate including mass transport, electron transfer, electrical potential, chemical potential and crystal growth [85]. In metal deposition, for example, an ion must reach the electrode/solution interface (mass transport), receive electrons (electron transfer) and then join other atoms to form a crystal (crystallization). The aim of this Chapter is to give some insight into the mechanisms affecting localized electro-chemical deposition. Rigorous quantitative theoretical and experimental analysis of rate limiting mechanisms and deposition profiles is left to future work.

### 3.2 Deposition Rate

Conventional electroplating rates are too slow to make a localized electro-chemical deposition process feasible. Study of the limiting processes, however, suggests means of en-

Figure 3(a): The SCMED Concept.

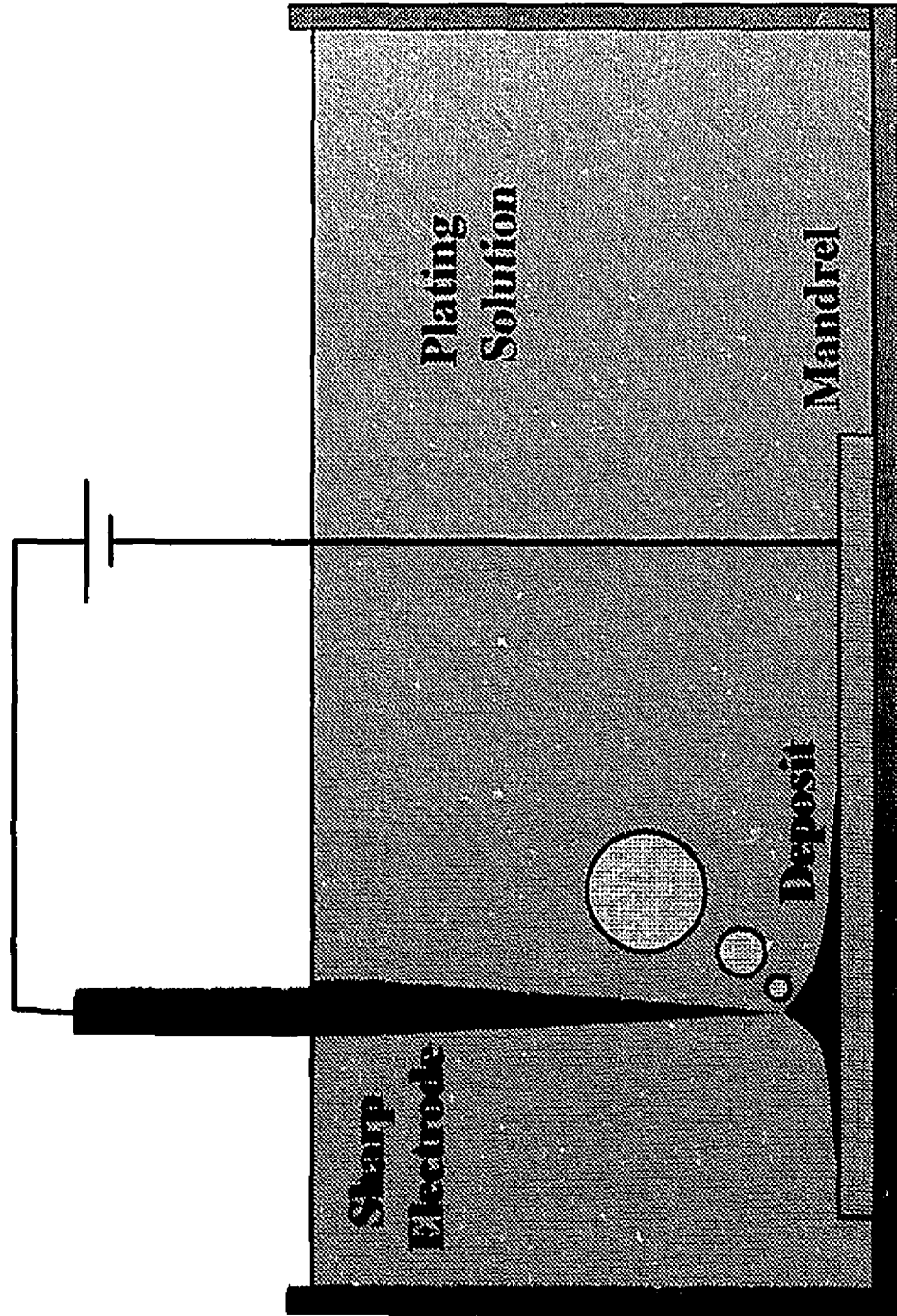
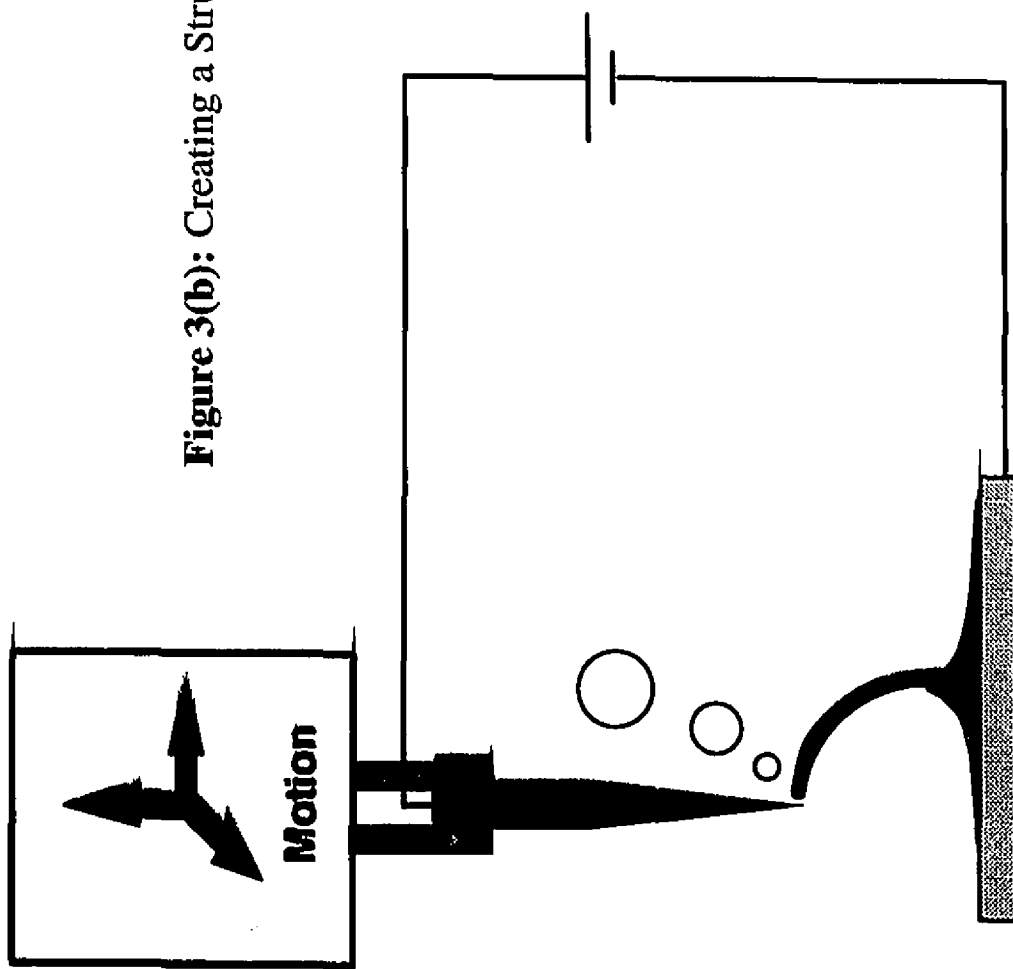


**Figure 3(b):** Creating a Structure using SCMED.

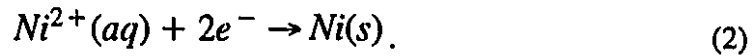


hancing rate. Electron transfer and mass transport are generally the main factors affecting the rate of electrodeposition. Electro-crystallization is important to the structure of the deposit [85].

In the following discussion deposition rate and current density are used interchangeably. The current density,  $j$ , due to a particular chemical species being deposited at an electrode is in fact directly proportional to the vertical deposition rate,  $F_v$  [m/s]:

$$j = \frac{\rho N_A z e}{m} F_v \quad , \quad (1)$$

where  $\rho$  is the density of the material deposited,  $N_A$  is Avagadro's number,  $z$  is the ionic charge of the species in solution,  $e$  is the elementary charge, and  $m$  is molar mass. Equation (1) is easily understood by realizing that the deposition of an atom (or molecule) involves the a charge transfer of  $z$  electrons. In the case of nickel for example:



### 3.2.1 Electron Transfer

At equilibrium a balance between chemical and electrical potential occurs at the electrode/solution interface manifesting itself as <30 nm thick charged region known as the double layer [86]. To achieve electron transfer an activation energy is required for an ion or molecule to rid itself of solvating molecules, travel through the double layer and adjust its hydration sphere for electron transfer [87]. An equal energy is required for atoms and molecules leaving the surface, and a dynamic equilibrium exists with oxidation and reduction currents matching each other. If the electrical potential is changed from the equilibrium value by an amount,  $\eta$ , either reduction or oxidation is favoured, as described by the semi-empirical Butler-Volmer equation [86]:

$$j = j_o [e^{(1-\alpha)\eta} - e^{-\alpha\eta}] \quad , \quad (3)$$

where

$$f = \frac{F}{RT} ,$$

and  $j$  is current density,  $j_0$  is exchange current density (the absolute value of the oxidation or reduction current at equilibrium for given electrode concentrations of reactants),  $F$  is one Faraday ( $9.6485 \times 10^4 \text{ C}\cdot\text{mol}^{-1}$ ),  $R$  is the gas constant ( $8.31451 \text{ J}\cdot\text{K}^{-1}\text{mol}^{-1}$ ),  $T$  is the absolute temperature, and  $\alpha$  is an experimentally derived parameter known as the transfer coefficient, which lies between 0 and 1 and is usually  $\approx 0.5$ . Once overpotential exceeds  $\approx 100\text{mV}$  the rate of transfer rises exponentially (assuming  $\alpha=0.5$ ). At the potentials used in electroplating and forming, electron transfer rates generally greatly exceed those of mass transport. The concentration of the reactant is thus reduced near the electrode and mass transport is the rate determining step.

### 3.2.2 Mass Transport

The three mechanisms of mass transport are diffusion, migration and convection. Diffusion is driven by concentration gradients ( $\nabla C$ ), migration by the action of electrical potential gradients on charges ( $\nabla\phi$ ), and convection by density gradients or forced flow [86]:

$$\mathbf{J} = -D\nabla C - \frac{zF}{RT}DC\nabla\phi + C\mathbf{v} , \quad (4)$$

where  $D$  is the diffusion coefficient,  $\mathbf{v}$  is fluid velocity and  $\mathbf{J}$  is the flux of a given species ( $\text{mol s}^{-1} \text{ m}^{-2}$ ). (At an electrode, Equation (4) corresponds to a circuit current of  $j=nFJ_{\perp}$ , assuming that the electrode kinetics are much faster than the mass transport.  $J_{\perp}$  represents flux perpendicular to the electrode surface.)

#### 3.2.2.1 Diffusion

In conventional electroplating and forming diffusion is the rate determining process [88]. The concentration gradients created by the much more rapid process of electron transfer at the electrode induce diffusion. Rates of diffusion can be increased by reducing electrode diameter. The depleted volume has a cubic dependence on diameter while the surface

area decreases only with the square. Diffusion current density is thus a function of electrode radius,  $r_o$ , as well as the diffusion coefficient,  $D_o$ , bulk concentration,  $C_o$ , and the number of electrons reduced or oxidized per molecule,  $n$  [89]:

$$j(r_o, t \rightarrow \infty) = \frac{nFD_oC_o}{r_o} \quad , \quad (5)$$

for a hemispherical electrode. The concentration,  $C$ , as a function of radius,  $r$ , at steady state is:

$$C(r, t \rightarrow \infty) = C_o(1 - \frac{r_o}{r}) \quad . \quad (6)$$

Current densities at disks and other micro-electrodes behave identically but with different geometry-related constants. Reducing the electrode diameter from 100  $\mu\text{m}$  to 0.1  $\mu\text{m}$  increases diffusion current by 1000 times. For a sulfamate solution for example, as used to build the nickel structures described below, this corresponds to a change in deposition rate from  $\approx 0.06 \mu\text{m/s}$  to  $\approx 60 \mu\text{m/s}$ , making localized deposition feasible using  $< 5 \mu\text{m}$  diameter electrodes (providing diffusion remains the rate determining process). Note that while vertical deposition rate is inversely proportional to electrode diameter, the rate of volume deposition is directly proportional to diameter for a diffusion limited process. In situations where fabrication rate is diffusion limited, one would ideally have a range of electrode sizes available to produce a range of feature sizes in the least time.

### 3.2.2.2 Convection

Depletion of ions near the electrode also creates density gradients between the depleted region and the electrode, resulting in natural convection. Agitation is often used to force convection, leading to the flow of bulk solution into the depletion layer, and increasing deposition rates by as much as 100 times [85]. However rates are still relatively slow. Rapid

nickel deposition rates at large area electrodes ( $\geq 10^{-2} \text{ mm}^2$ ), for example, are on the order of  $0.03 \text{ } \mu\text{m/s}$  [90]. At such rates a serial deposition process, as is proposed here, is impractical.

Agitation reduces the depleted region from an initial value of as much as  $500 \text{ } \mu\text{m}$  to  $\sim 10 \text{ } \mu\text{m}$  [91]. In spite of agitation, deposition remains diffusion limited because viscous forces near the electrode surface impede the influx of fluid. However, local heating of the surface can be used to create micro-stirring, bringing solution directly to the surface. A technique known as Laser Enhanced Electroplating (LEEP, see Section 2.3.6.2) takes advantage of this effect by focussing a laser beam onto the plating surface [70], apparently resulting in convection both by the inducement of micro-stirring and, with sufficient laser intensity, by local boiling. Rates of deposition and etching are enhanced by more than three orders of magnitude over rates in an unagitated solution. Two micrometer wide lines have been deposited using this process and equivalent vertical deposition rates of greater than  $6 \text{ } \mu\text{m/s}$  achieved. However LEEP appears to be impractical for three dimensional fabrication, as discussed in Section 2.3.6.2. Nevertheless, it demonstrates that flow at the surface can significantly increase deposition rates, as required for a serial deposition process to be successful.

### 3.2.2.3 Migration

The current density due to migration of a species in solution is proportional to the electric field,  $E$ , by Ohm's law [86]:

$$j = \sigma E \quad , \quad (7)$$

with

$$\sigma = zuCF \quad , \quad (8)$$

where  $\sigma$  is conductivity,  $u$  is the ionic mobility, and  $z$  is the ionic charge. All charged species in solution are acted upon by the field, irrespective of whether they are involved in deposition

or not, the proportion of current carried by a given species being specified by its transport number [86]. In conventional electrochemical configurations, migration generally plays a secondary role in mass transport to the depleted region because much of the current is carried by ions of species that do not react. In sulfamate solution, the Nickel plating bath used to grow the structures presented below, the Ni ion transport number is  $\approx 0.25$ . Diffusion and convection must carry the remaining portion of the current to the electrodes.

When the field is localized using a microelectrode, very strong fields result. This allows very high local rates of migration, but does not contribute to the influx of ions to the region between the microelectrode and the substrate, and thus may in effect contribute to depletion, adding to the dependence on other forms of mass transport.

### **3.2.2.4 Electro-Crystallization**

Electro-crystallization involves a phase conversion in which ions form solids. Once the ions reach the electrode surface and electron transfer takes place, resulting in neutral species, several steps remain [85]. The first step is to rid of the solvation sheath. In aqueous solution the sheath is composed of water molecules, whose polar nature attracts them to ionic charge. Next, surface diffusion takes place as the adsorbed atom seeks an energetically favourable spot to rest. On foreign substrates or smooth surfaces the atoms cluster to form nuclei. These become stable once they reach a size such that the bulk free energy dominates over surface tension, and thus reduces free energy. Subsequently, atoms diffuse to lattice sites and lattices grow to develop the crystallographic and morphological properties of the deposit.

Electro-crystallization is a complex process for which analytic models tend to be of a qualitative nature [85]. It is generally not the rate limiting process; However, electro-crystallization does determine a deposit's material properties.

### 3.2.3 Deposition Profile

In this section a the deposition profile produced by SCMED is modelled. Modelling was originally done to determine the extent of field localization due to a micro-electrode placed near a surface, and thus to assess the feasibility of the SCMED concept.

Deposition profile refers to the geometry of the deposit produced by a given electrode configuration. In order to determine the deposition profile, the current density at the substrate surface must be calculated. This involves solving for mass transport, electron transfer, double layer impedance and the distribution of electrical potential,  $\Phi$ . I chose to begin with an estimate of the field distribution at the substrate due to a nearby microelectrode since the electrical potential drives the electrochemical reaction, and thus localization of electric field is the key to the localization of deposit.

The distribution of electrical potential is given by Poisson's equation [92]:

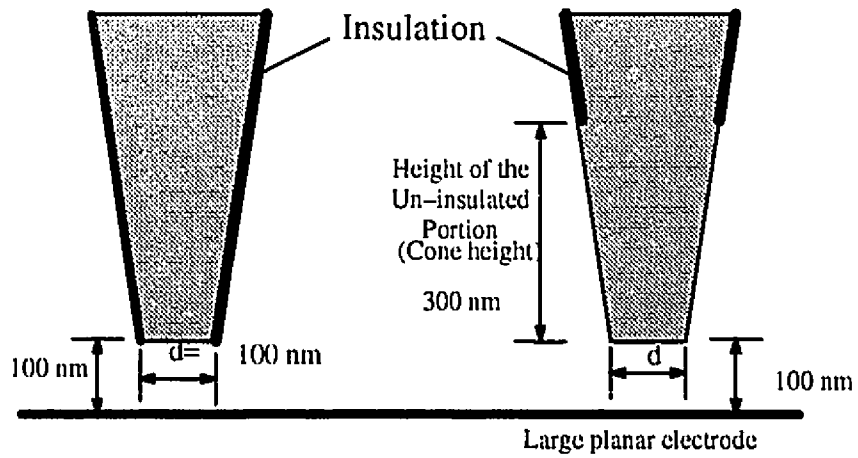
$$\nabla^2\Phi = -\frac{\rho}{\epsilon_0} \quad (9)$$

In this case  $\rho$  represents charge density and  $\epsilon_0$  is the permittivity of free space ( $8.85 \times 10^{-12} \text{ C}^2/\text{N}\cdot\text{m}^2$ ). In order to estimate the shape of the field it is assumed that there is no net charge and the problem is reduced to solving Laplace's equation. The actual field profile will be distorted by double layer charging, and the charging will tend to be greatest where the field is strongest, leading in turn to a spreading of the field. Thus the model represents a best case. The double layer is generally on the order of a nanometer thick [88] and certainly less than 30 nm across [86], so the approximation is likely a reasonable one given an electrode separation of  $\geq 100$  nm.

Microelectrode geometry is modelled on electrochemically etched electrodes such as those used for scanning tunneling microscopy [93] and scanning electrochemical microscopy [94]. The etched tips generally have a conical shape converging to an approximately dis-

Case 1: Disk

Case 2: 300 nm cone.



Case 3: 1000 nm cone.

Case 4: 5000 nm cone.

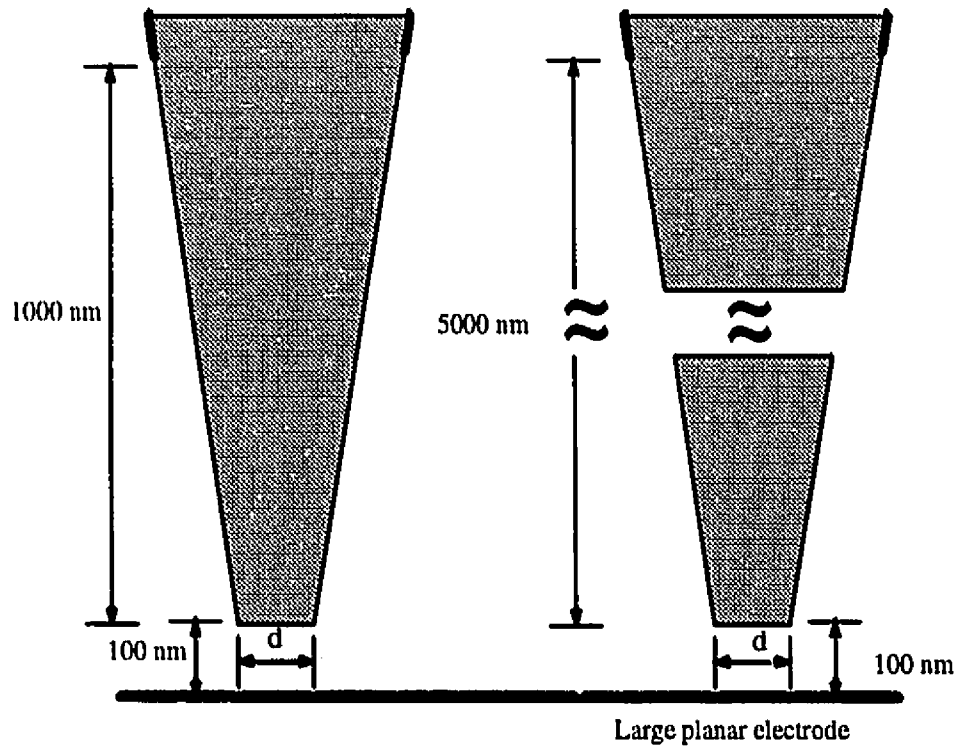
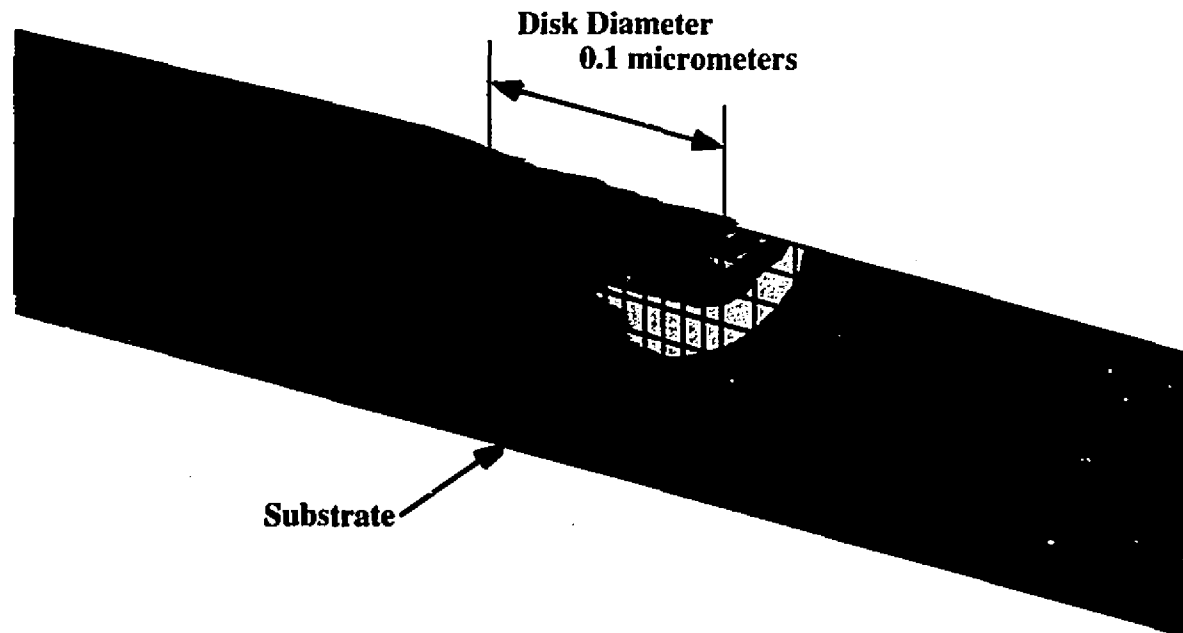


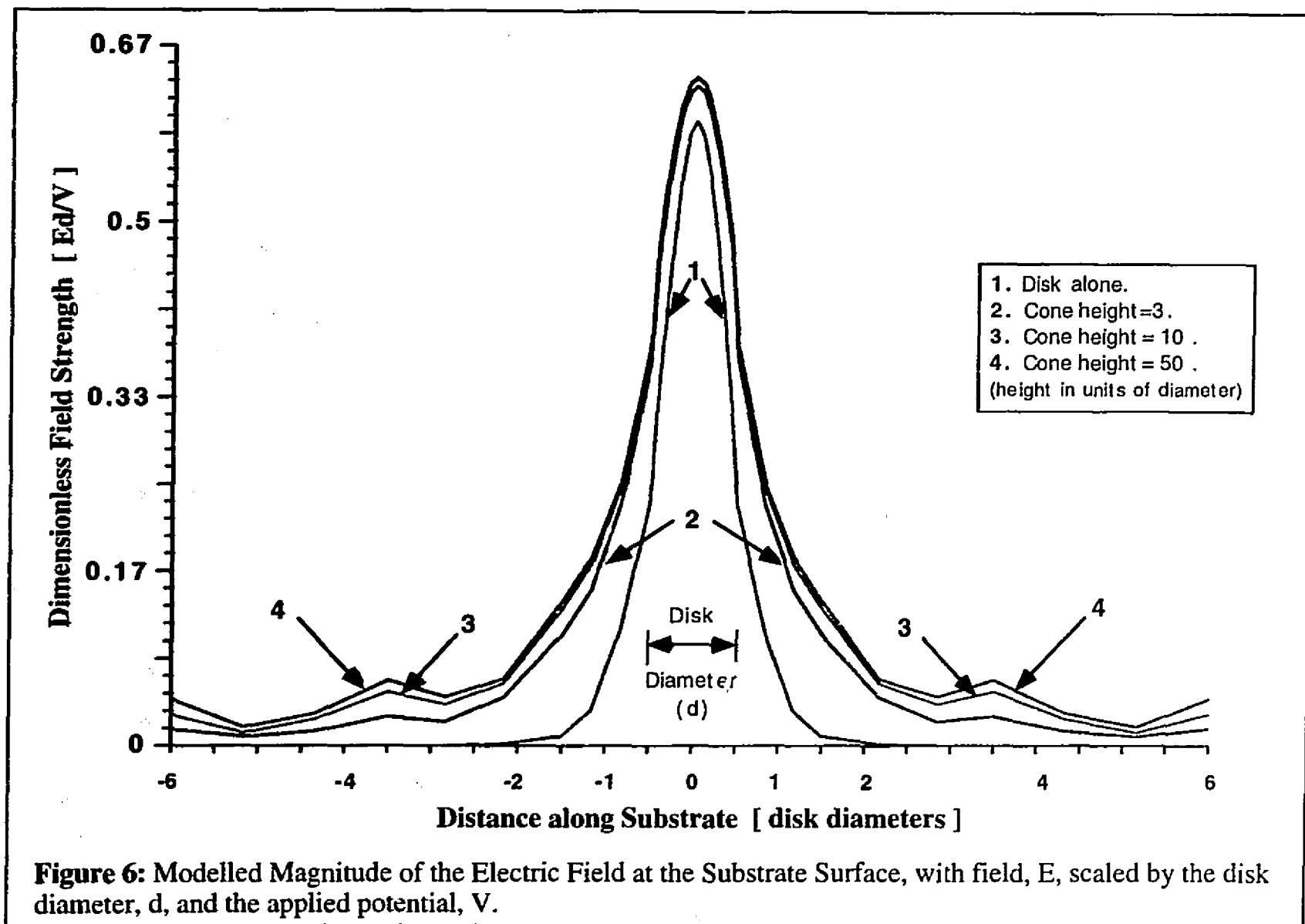
Figure 4 : Modelled Electrode Tip Geometries. Dimensions are examples. The modelled results are dimensionless.

coid or hemispherical point, as shown in Figure 4. Two electrode configurations are modelled, one in which insulation covers the length of the electrode, leaving only a 100 nm diameter disk shaped tip exposed, and secondly a configuration in which a portion of the conical segment above the disk is left uninsulated. The cone angle is 28 degrees, the value chosen to be representative of cone angles observed in etched tips. The model assumes that the disk electrode sits one disk diameter above and parallel to a much larger planar electrode for all tip configurations. This separation is chosen because the current at micro-electrodes begins to rise from its bulk value as it approaches within a disk diameter of a large planar surface [95], possibly providing feedback for future servo control of tip position. A potential difference is applied between the microelectrode and the plane. Between the two lies a medium of constant conductivity. Calculations were done using a finite element modelling package (MacNeal/Schwendler EMAS [96]). Dimensional analysis demonstrates that electric field results are valid for all configurations exhibiting geometric similarity, given that charging can be neglected.

Figure 5 shows the calculated field strength for a perpendicular cross-section through the plane and the microelectrode (in the disk configuration). Note that the highest fields occur at the edge of the microelectrode, as expected. In Figure 6, the field strength profile along the plane's surface is plotted for both the disk configuration and for cone heights that are 3, 10 and 50 $\times$  disk diameter. The full width at half maximum (FWHM) ranges between 1.5 $\times$  the disk diameter for the disk alone, and  $\approx 2\times$  for the 10 and 50 $\times$  cones, demonstrating that the field is effectively localized under the modelled conditions. Furthermore, profile broadening appears to be converging as cone height is increased, as expected given that spreading of the field lines and the resistance both increase the further an electrode surface is from the substrate. Thus even sharp uninsulated electrodes should be effective in providing field localization.



**Figure 5 :** Modelled Cross-Section of Current Density between a Disk and a Planar Substrate. Contours are linearly spaced representing a variation in field strength of 150 times, the strongest fields being at the disk edges. Grid lines delineate the borders of the elements used.



### 3.3 Summary of Theory

Deposition rate and profile are critical to the success of SCMED. Mass transport is generally the rate determining factor in conventional electroplating and forming, limiting deposition rates to magnitudes that are too slow to make SCMED feasible. Two methods exist which can potentially increase deposition rate. The first is to reduce electrode size, resulting in an increase in diffusion current density inversely proportional to electrode dimensions. Analysis suggests that reasonable rates should begin to occur at electrode dimensions of  $\leq 5\mu\text{m}$ . The second alternative is to induce convection. Results from laser enhanced electroplating suggest that currents induced by local heating can increase rates by  $>1000\times$ , and further increases are observed due to bubble formation at the onset of boiling.

Electric field distribution, which in turn affects deposition profile, was modelled, demonstrating that in the "best case" of negligible double layer charging, localization is achieved, and that a sharp conical tip need not be insulated in order to produce field localization. Localized electro-deposition employing STM tips has in fact been experimentally demonstrated by others in two dimensions, as described in Section 2.3.6.3, and in 3D, as shown in Chapter 6.

## Chapter 4 : The Forced Convection Approach

The concept of Spatially Constrained Micro–Electrochemical Deposition (SCMED) has evolved since its conception. In the initial configuration the localization of field is accompanied by the injection of fresh plating solution. Here we discuss the original design, its advantages and the problems that led to the elimination of the forced convection aspect for the time being. The forced convection approach is very elegant and may eventually prove to be the best, once its drawbacks are overcome.

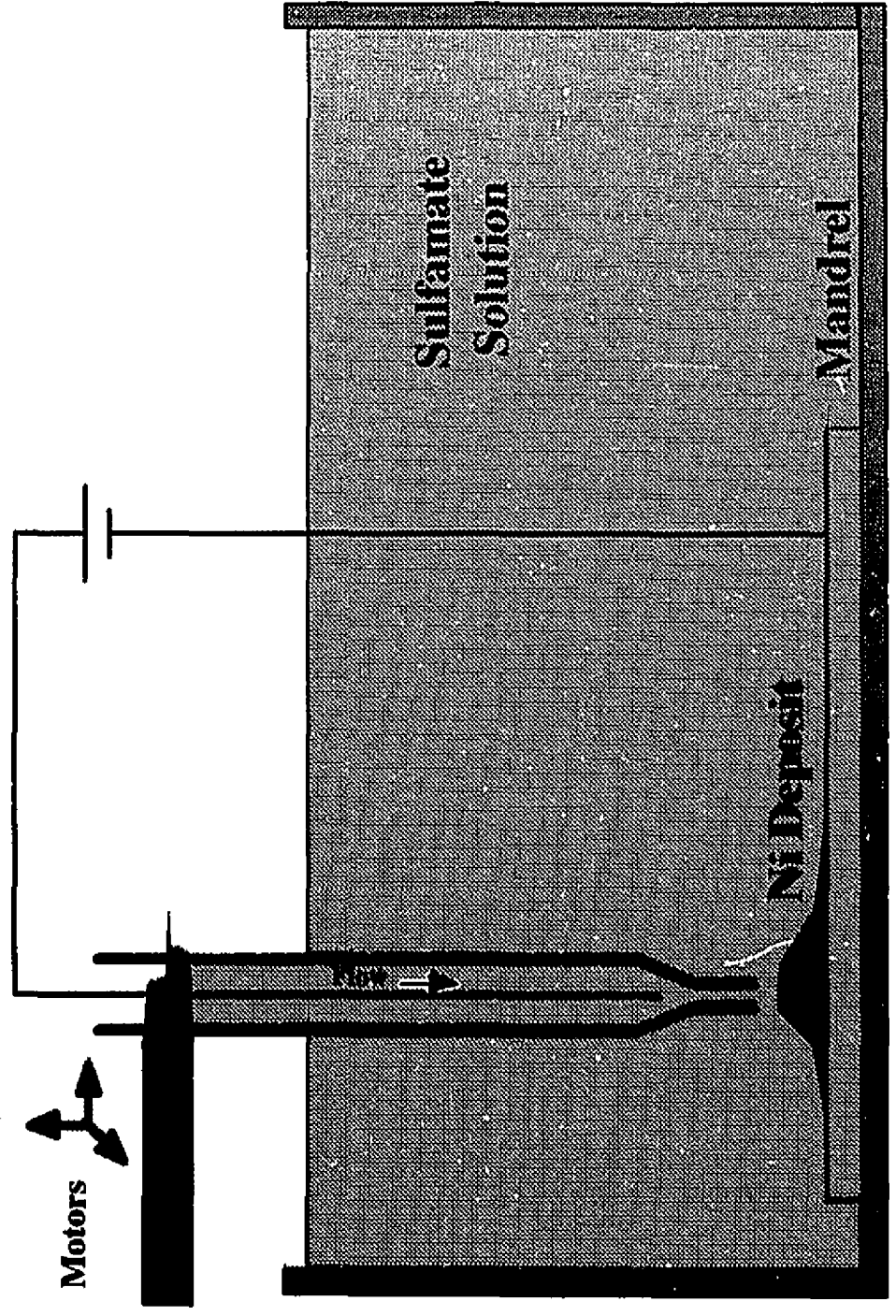
The chapter begins with a discussion of the concept of forced convection SCMED. A low resolution (100  $\mu\text{m}$ ) prototype built to test the concept is described. Calculations investigating the feasibility of scaling resolution down to the sub–micrometer scale are presented. Obstacles related to control problems and scaling are discussed, as are approaches for overcoming these difficulties.

### 4.1 Spatially Constrained Micro–Electrochemical Deposition and Forced Convection

The forced convection concept is shown in Figure 7. It involves field localization, as in the approach presented in Figure 2. Unlike the concept described in Figure 2 concentrated plating solution is injected directly into the deposition region. As discussed in Chapter 3, deposition rate is generally diffusion limited. The flow of solution is intended to remove mass transport limitations and thereby greatly enhance deposition rate. At very high flow rates it might also be possible to rid of the solvation sheath as the depositing ion is blasted towards the deposition surface, thus reducing activation energy.

A pipette can be used to direct the flow, and pipettes have been fabricated having orifice diameters of < 100 nm [97]. The field pattern between the pipette tip and the substrate will

Figure 7: SCMED with Forced Convection.



be directed through the orifice and thus will behave similarly to a disk electrode. Deposition rate is now related to flow.

#### **4.1.1 Implementation**

The forced convection apparatus is represented in Figure 7. Plating solution is forced down a pipette by applying pressure using a low solubility gas such as argon. An electrode sits within the pipette and a potential is applied between it and a conducting substrate. The pipette is then moved appropriately with respect to the forming surface in order to produce structures.

In implementing the scheme, plating solution was chosen on the bases of achievable uniformity, strength and residual stress of the deposit. Nickel deposits from a sulfamate solution to produce high tensile strength (415–620 MPa), low internal stress (0–55 MPa) deposits with sub–micrometer uniformity [98]. A combination of sulfamate and nickel chloride is also suitable.

The pipette used must be able to withstand the pressures exerted by the fluid and reach sub–micrometer orifice sizes. Quartz is the ideal material given its high tensile strength and range of elastic deformation. However, quartz pipettes are somewhat more difficult to construct than those made of glass because the very high softening temperature (1660°C) cannot be reached using conventional resistive heaters alone. Attempts were made at softening quartz using a 10 W CO<sub>2</sub> laser beam focussed on a 1mm diameter tube, but the power was insufficient. Thus, to begin with, glass pipettes were used, which are readily available with micrometer sized orifices, and for which nanometer sized orifices are achievable [97].

Platinum wire was chosen as the pipette electrode material. Platinum has very low polarizability, implying high exchange currents, (Equation (3)) and thus high rates of electron transfer. The electrodes were inserted through the pipette wall near the tip. 300 μm diameter holes were etched by locally dissolving the glass in a 30% by weight aqueous solution of NaOH. The etching is achieved by bringing a needle into contact with the glass (or quartz)

and applying a potential ( $\approx 35$  V) between the needle and the solution. Local heating induced by sparking apparently changes reaction kinetics sufficiently to favour the rapid dissolution of the glass [99][100]. Bonding of the electrodes and plugging of the holes was performed using UV adhesive. Conventional micro-stepping motors and stages provided a large range of motion ( $\geq 60$  mm) and small step size (20 nm).

Using these materials, including glass pipettes with orifice diameters on the order of 100  $\mu\text{m}$ , nickel deposits were successfully formed. In order to produce structures, however, some feedback is required to determine orifice position relative to the forming surface. Also, the effects of scaling down the orifice diameter to sub-micrometer dimensions on the pressures required to induce flow, and on the electrical resistance, needed to be considered.

## 4.2 Scaling Effects

### 4.2.1 Model of Pressure Drop in Flow through a Pipette

Given that the rate of deposition is dependent on the transport of ions and thus the flow, the required average flow speed at the pipette outlet,  $u_o$ , can be calculated for a given vertical deposition rate,  $F$ , and concentration,  $C$  [mol/L]:

$$u_o = \frac{\rho}{\alpha m C} F, \quad (10)$$

where  $\rho$  is density,  $\alpha$  is the proportion of in-flowing ions that are deposited and  $m$  [g/mol] is molar mass. A pressure drop must be applied to produce the flow. In this section the effect of scaling down pipette dimensions on the pressure required to drive the fluid is estimated.

First, the shape of the pipette must be described. In a micro-pipette there is generally a region where, starting from the tip, the radius,  $R$ , increases very gradually from its value at the orifice,  $R_o$ . This region is modelled by a linear change in radius:

$$R = R_o + \beta z, \quad (11)$$

where  $\beta$  represents the slope of the pipette wall and  $z$  is the distance along the axis from the

orifice. Even for a relatively short tipped pipette, with a steep slope, the diameter might only change from about 100 nm to 100  $\mu\text{m}$  over  $\approx 2$  mm, resulting in a slope  $\beta \approx 0.05$  [97]. At some point the slope will begin to change rapidly and the linear approximation no longer applies, but by that time the diameter is often sufficiently large that the pressure drop is negligible compared to that at the pipette tip. The variables used to describe the pipette geometry are shown in Figure 8. Length,  $L$ , represents the length over which radius increases linearly.

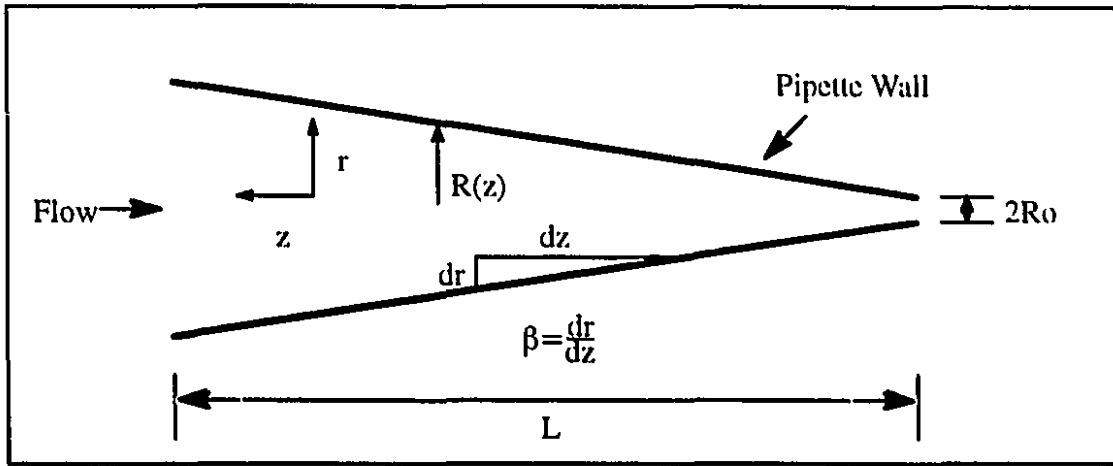


Figure 8 : Variables in the Pipette Flow Calculation.

The induced pressure drop can be calculated from the Navier–Stokes equations using the lubrication approximation [101]. The approximation essentially assumes that the changes in geometry along the direction of flow are sufficiently gradual that these changes need not be accounted for in calculating the flow profile at any given cross–section. For flow through the cylindrically symmetric pipette tip, for example, it is assumed that:

$$\frac{\partial^2 v_z}{\partial r^2} \gg \frac{\partial^2 v_z}{\partial z^2}, \quad (12)$$

where  $v_z$  is the velocity along the axis of symmetry, and also that:

$$\frac{\partial P}{\partial r} \ll \frac{\partial P}{\partial z}. \quad (13)$$

Relations (12) and (13) hold for the small  $\beta$  values found in most pipette tips.

The velocity profile for fully-developed, laminar and incompressible flow in a tube can now be used [102]:

$$v_z(r) = 2u(z) \left[ 1 - \left( \frac{r}{R(z)} \right)^2 \right] \quad (14)$$

where  $u(z)$  is the average flow speed. From the velocity profile, the pressure gradient is found to be:

$$\frac{\partial P}{\partial z} = \frac{8\mu u(z)}{R(z)^2} \quad (15)$$

where  $\mu$  is the solution viscosity. Note that flow speed and pipette radius are functions of distance along the tube.

Since the volume of flow is constant through any pipette cross-section, the average flow rate at any position,  $z$ , can be related to the flow rate at the orifice:

$$u(z)R^2 = u_o R_o^2 \quad (16)$$

The total pressure drop is found by substituting for  $u(z)$  in Equation (15) (from Equation (16)) and for  $R(z)$  (from Equation (11)) and integrating over the length of the narrow region:

$$\Delta P = \frac{8\mu u_o}{3R_o\beta} \left[ \left( 1 + \frac{\beta L}{R_o} \right)^{-3} - 1 \right] \quad (17)$$

The term in square brackets can be neglected when  $\beta L \gg R_o$ . Since  $L$  is generally on the order of a few millimeters or more, and  $\beta \approx 0.1$ , the bracketed term is essentially unity for pipettes with orifices  $\leq 10 \mu\text{m}$ ; The pressure drop is then simply inversely proportional to orifice diameter.

Assuming an optimistic vertical deposition rate of  $60 \mu\text{m/s}$  using a pipette with an orifice diameter of  $100 \text{ nm}$ , and that only one in 5 flowing ions are deposited (the actual ratio is unknown, but should be low given high rates of electron transfer), the required exit velocity,

$u_o$ , is  $\approx 0.05$  m/s. Using a sulfamate plating solution and a slope,  $\beta = 0.05$ , the required pressure drop is  $\Delta P \approx 60$  kPa, less than one atmosphere. Such a pressure is easily achievable. (The Reynold's number for this flow ranges between  $\approx 50$  at the inlet to  $\approx 0.005$  near the orifice, and thus flow is clearly laminar.)

If all the pressure is concentrated at one point in the pipette, the ratio of wall thickness,  $t$ , to radius required to withstand it is determined by tensile strength,  $T$ :

$$\frac{t}{R} = \frac{\Delta P}{T} \quad (18)$$

For quartz ( $T = 50$  MPa) and all glasses normal wall thicknesses easily withstand the applied pressure.

If the model of pipette geometry is incorrect and the diameter in fact stays constant for a length of even  $500 \mu\text{m}$ , enormously large pressure drops are required, on the order of a  $10$  MPa. These calculations have not yet been experimentally verified, and were simply done to determine whether forced convection through a pipette might be feasible.

## 4.2.2 Electrical Resistance and Potential Drop

The next step is to determine how the electrical potential drop across the tip scales. Potential drop,  $dV$ , across a length of pipette,  $dz$ , is given in terms of conductivity,  $\sigma$ , and current density,  $J$ , by Ohm's Law (Equation (7)):

$$dV = \frac{J(z)}{\sigma} dz \quad (19)$$

Current density at the orifice,  $J_o$ , may be approximately expressed in terms of vertical deposition rate:

$$J_o \approx \frac{ezN_A Q}{tm} F_v \quad (20)$$

where  $e$  is the elementary charge,  $z$  is ionization number,  $t$  is transfer number (the proportion of current carried by the ion being deposited), and  $N_A$  is Avagadro's constant. The relation

is only approximate because the current at the orifice will result in a deposit area that is larger than that of the orifice. (Equation (20) is exact when the deposit and the tip areas are identical.)

Current is conserved as it travels down the pipette, and therefore:

$$J(z)R^2 = J_oR_o^2 \quad (21)$$

The potential drop,  $\Delta V$ , is found by integrating Equation (19) over the pipette length, with the  $z$  dependence of current density being provided by the combination of Equations (21) and (11), yielding:

$$\Delta V = \frac{J_oR_o}{\beta\sigma} \left[ 1 - \left( 1 + \frac{\beta L}{R_o} \right)^{-1} \right] \quad (22)$$

The potential drop in fact decreases in direct proportion to orifice diameter for a given vertical deposition rate, for small  $\beta L/R_o$  (true in this case providing that  $R_o < 5 \mu\text{m}$ , assuming a length,  $L$ , of several millimeters). For a deposition rate of  $60 \mu\text{m/s}$ , and using the conductivity value determined experimentally in Section 6.3, with an orifice diameter of 100 nm, the potential drop  $\Delta V = 42V$ . The dielectric strength of quartz is  $8\text{MV/m}$ , so the minimum pipette wall thickness near the tip to withstand such a potential drop is:

$$t = \frac{V}{V_b} = 5\mu\text{m} \quad (23)$$

The wall thickness to inner diameter ratio is about 50. Glass tubes such as those used in Hg thermometers have similar ratios.

The analysis of pressure and potential drop suggests that inducing forced flow of solution through a pipette is feasible down to the sub-micrometer scale.

## 4.3 Deposition Control

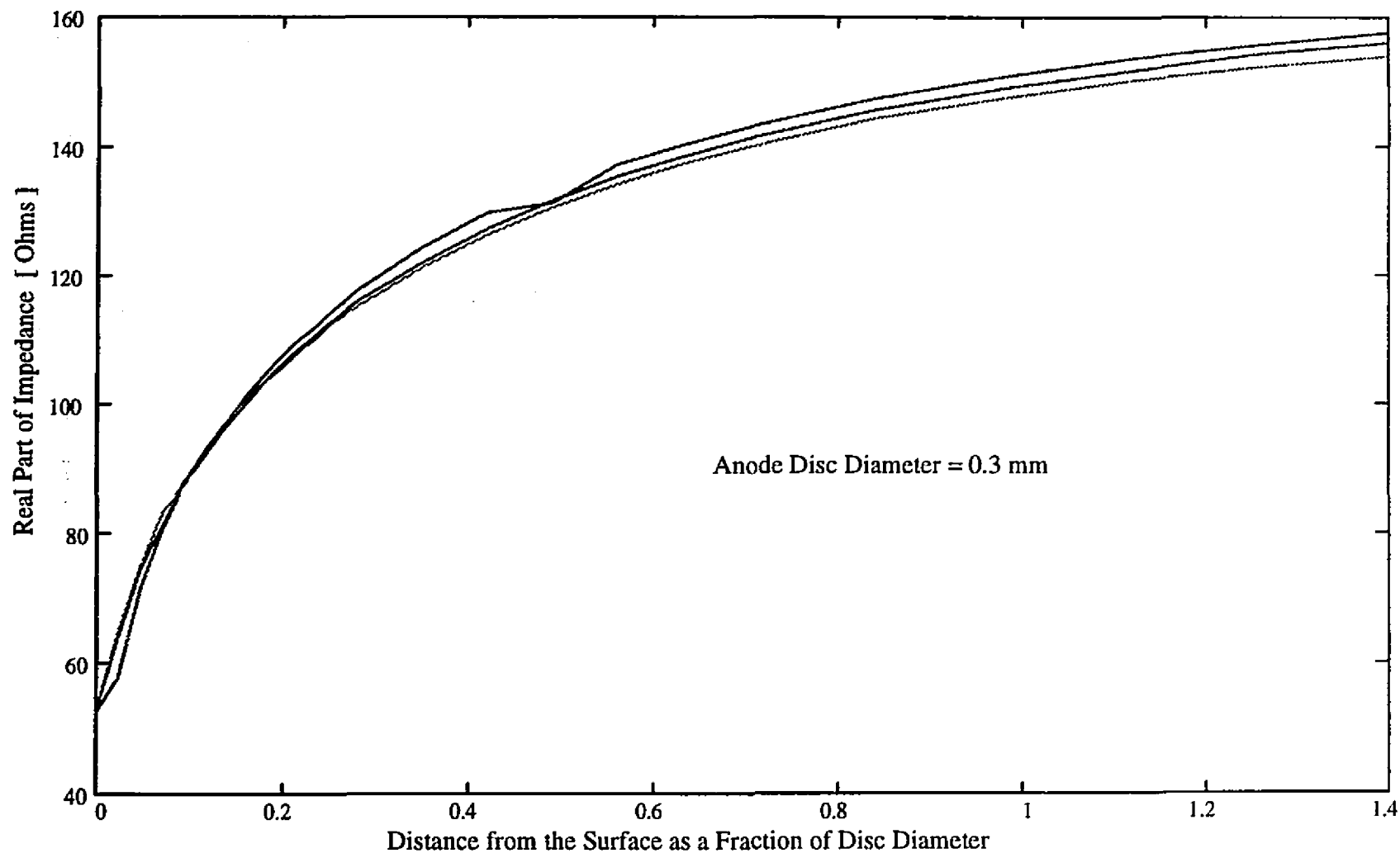
The tip to substrate distance determines the field geometry and hence the deposition profile. It is critical that this distance be controlled in order to build structures.

Work by Allen Bard and his colleagues on scanning electrochemical microscopy has demonstrated experimentally that tip to substrate separation is related to steady state current [80][94]. Unfortunately, significant increases in current are observed only within one tip diameter of the substrate. As stated in Section 2.3.6.3, this was one of the reasons they abandoned deposition from aqueous solution and used thin polymer films. A further difficulty is that at the potentials required to produce significant deposition rates, hydrogen and oxygen are also evolved. The resulting bubble formation results in large current fluctuations, making the averaging of current over time necessary (bubble formation has a characteristic frequency of a few Hz).

After many lost pipettes, investigation was done to see if any other means of determining tip to substrate distance was available. Bard used DC currents, but AC currents were not tried. Using an impedance analyzer (HP4194A) scanning between 100Hz and 40MHz it was found that the maximum variation in impedance as a function of separation occurred at 3MHz. The impedance – displacement relationship at 3MHz is shown in Figure 9. It was obtained using a 300 $\mu$ m diameter platinum disk electrode (a 300  $\mu$ m insulated Pt wire) which was brought to the surface and then displaced vertically in 7  $\mu$ m increments. The disk was used rather than a pipette so that contact with the deposition surface was clearly recognizable. The experiment was done in sulfamate solution. As in Bard's results, useful variation essentially occurs only within one disk diameter. Note that the curves were obtained at voltages where gas evolution did not occur, reducing noise due to bubble formation. Unfortunately, deposition rates are too slow at such potentials ( $\leq 0.05 \mu\text{m/s}$ ).

Current feedback may also be obtained by making use of deposit growth. If an electrode is left stationary, the deposit eventually makes contact, producing a step rise in current which

**Figure 9:** Measured Real Part of Impedance at 3 MHz as a Function of Tip to Substrate Distance – 3 Trials



can be used for simple position control. For this to work the electrode surface must be able to make contact with the surface, and thus be at the end of the pipette. Tip resistance would also be eliminated by moving the electrode right to the tip. The drawback is that such a scheme is somewhat difficult to build and would likely worsen resolution for a given sized pipette orifice.

#### 4.4 Magneto–Hydrodynamic Flow

The aim of forced convection is to bring concentrated solution as close as possible to the electrode surface, and thus to increase mass transport rates. Clearly, the injection of fresh plating solution is not the only means of forcing convection. Solution agitation is another possibility. To this end Magneto–Hydrodynamic (MHD) induced flow was tried.

The magneto hydrodynamic effect is the manifestation of the Lorentz force in a conducting solution. Ions in solution are acted upon by perpendicular electric ( $E$ ) and magnetic ( $B$ ) fields, resulting in a force,  $F$ , given by the Lorentz force law [92]:

$$F = Q[E + (v \times B)] \quad , \quad (24)$$

where  $Q$  is the ionic charge and  $v$  is ion velocity. If the fields are uniform a cycloid motion results, where the net displacement of both positive and negative ions is in the same direction, and at right angles to the  $E$  and  $B$  fields. The ions pull their solvation spheres with them, creating a flow. This effect has been applied to build angular accelerometers and to generate power from tidal flows.

In the MHD configuration, two relay electromagnets are used to produce magnetic fields of up to 0.5 Tesla. A 300  $\mu\text{m}$  diameter platinum disk was used as the micro–electrode in place of the pipette/electrode combination. The magnetic field is arranged to be perpendicular to the micro–electrode to substrate electric field. Flows on the order of 10 mm/s are possible. Neodymium Iron Boron magnets also serve to generate  $B$  fields.

Experiments compared currents generated with and without applying a magnetic field. Unfortunately no significant differences were found. Once voltages become sufficient to generate rapid flow, gas evolution is vigorous. It may be that the bubbling generates as much or more convection on the surface as the MHD flow.

## **4.5 Deposition without Forced Convection**

The MHD experiments demonstrated that high current densities ( $>10^5 \text{ A/m}^2$ ) are achievable without forced convection when potentials at which vigorous gas evolution occurs are applied. Much of the current is due to hydrogen ions, but significant quantities of nickel are also deposited. The next Chapter describes the implementation of SCMED without forced convection, while Chapter 6 presents structures built using this approach.

## Chapter 5 : Experimental Methods

This chapter describes the apparatus and procedures involved in constructing the structures presented in Chapter 6. The method does not involve forced convection.

Figure 10 is a schematic of the experimental configuration. Nickel structures are formed from a sulfamate solution [88],  $\text{Ni}(\text{SO}_3\text{NH}_2)_2$  : 450g/L,  $\text{H}_3\text{BO}_3$  : 30g/L (Aldrich, Milwaukee) onto nickel and copper mandrels. Mandrel surfaces are buffed (felt buffing wheel) or mounted in bakelite and mechanically polished in stages, beginning with 600 grit paper, followed by 25  $\mu\text{m}$  alumina powder and finally using 0.3  $\mu\text{m}$  alumina powder. The buffed surfaces are washed with soap and distilled water, rinsed in water, dipped in concentrated HCl, re-rinsed, then immediately immersed in the sulfamate solution. Polished surfaces are rinsed with water and ethanol before immersion in the sulfamate bath.

300  $\mu\text{m}$  diameter platinum wires are electrochemically etched in a solution of saturated NaCl (36% by volume), HCl(4%) and water(60%) [103] against a graphite rod at 22 V RMS to form conical tips with 10 to 100  $\mu\text{m}$  diameter heads. Etched and glass coated Pt:Ir (70:30) electrodes with tip diameters between 1 to 5  $\mu\text{m}$  (FHC Corp., Brunswick ME) are also used. Current measurements done in the sulfamate solution before and after subjecting the coated tips to a 5 V potential show an increase in current of up to 100  $\times$ , suggesting that the exposed electrode area increased, possibly resulting in a decrease in resolution.

Tips are translated in three dimensions using micro-stepping motors (Compumotor Corp., Rohnert Park CA) and stages (Design Components Inc, Medfield MA). The motors are driven by micro-step drives (AX series, 12,800 steps/revolution, Compumotor) allowing a 0.1  $\mu\text{m}$  step size on each axis. ASCII commands sent from a workstation (IBM RISC/6000) to the drives determine the trajectory. The operator interacts with a custom graphical user interface to specify geometry, Figure 11.

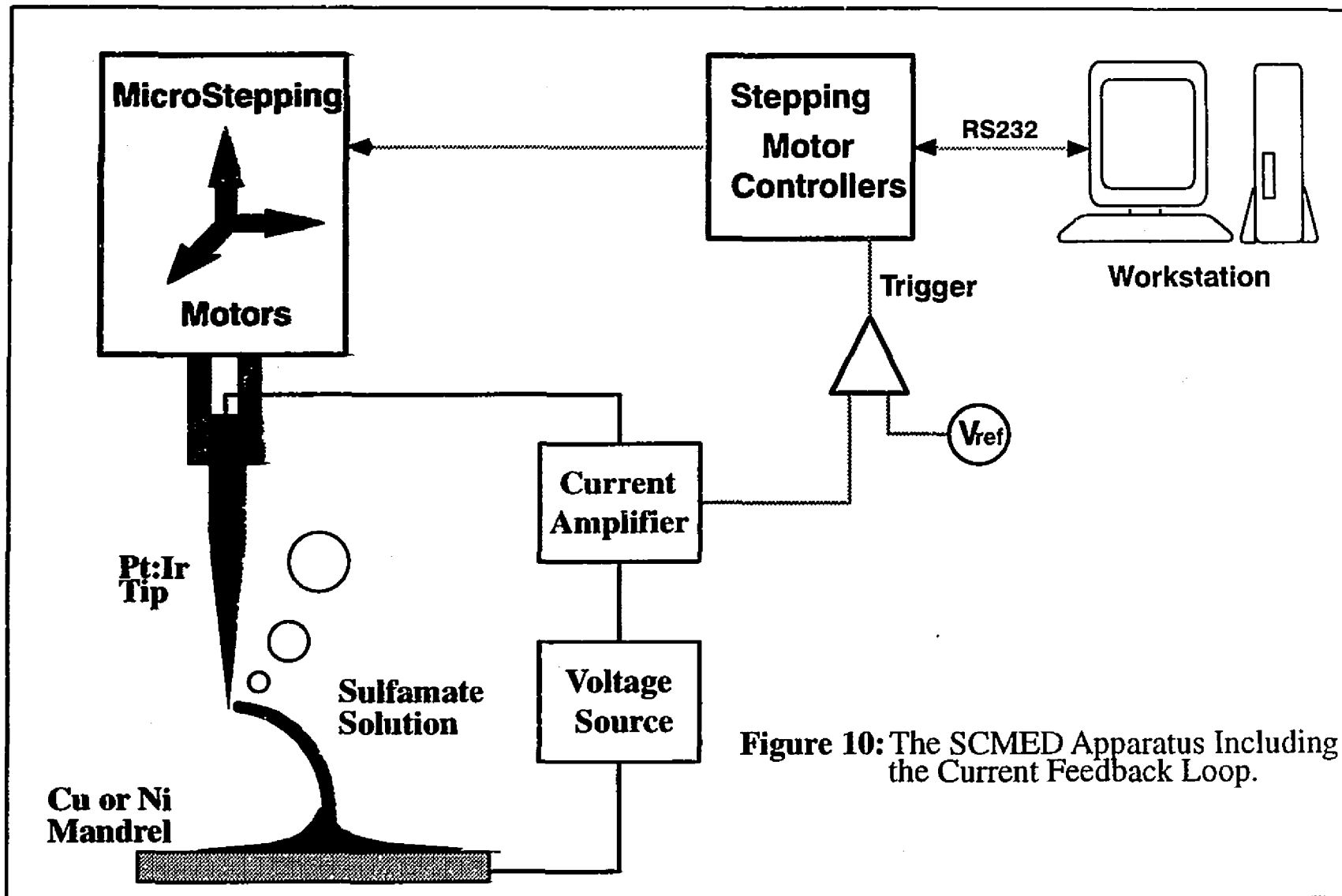


**Figure 10:** The SCMED Apparatus Including the Current Feedback Loop.

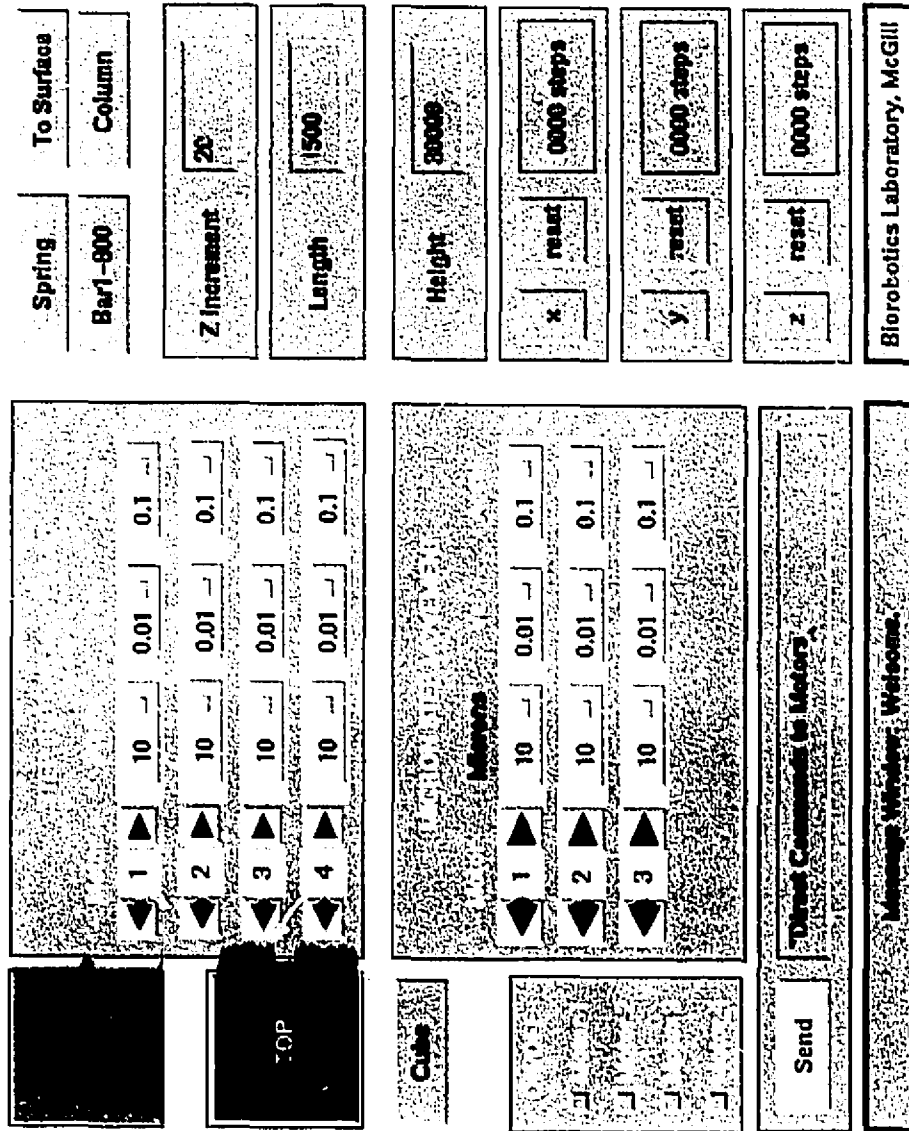


Figure 11 : The Custom Graphical User Interface used to control SCMED fabrication.

An  $\approx 5$  V potential is applied between the tip and the substrate in the sulfamate solution to induce rapid deposition. Higher voltages tended to produce powdery, black deposits whereas deposition rate drops off rapidly for potential differences of less than  $\approx 4.5$  V. In open-loop mode the tip velocity is constant. In closed-loop operation (Figure 10), current through the circuit is monitored (Keithley 428 current amplifier). Sharp rises in current (by  $\sim 100 \times$ ) indicate contact between the tip and the forming surface. These are used to trigger motion. Closed loop control is difficult using very fine uninsulated tips because of the high background current and therefore coated electrodes are used.

## Chapter 6 : Results

The merit of SCMED clearly depends on the structures it produces, the achievable resolution, the fabrication rate and the material properties of the deposits. Experimental results presented in this chapter demonstrate that three dimensional micro-structures can be built by SCMED at high deposition rates. X-ray diffraction and a stiffness measurements help identify material properties. It is also important to obtain an understanding the underlying mechanisms of the process. The determination of sulfamate solution conductivity presented here is one of the steps towards obtaining such an understanding.

### 6.1 Nickel Structures

Figure 12 is an electron micrograph of a nickel column 100  $\mu\text{m}$  high and 10  $\mu\text{m}$  in diameter. The structure stands on a copper substrate and was constructed in closed-loop mode using a glass coated electrode with a 3  $\mu\text{m}$  tip diameter. The tip was moved vertically from the surface under servo-control. Horizontal striations on the column are the result of time lags in the control mechanism used.

Figure 13 shows a nickel spring constructed by spiralling an uninsulated Pt electrode upward at a constant speed of 6  $\mu\text{m/s}$ . The deposition rate is two orders of magnitude higher than those of conventional nickel electroforming. Diffusion at a 100  $\mu\text{m}$  electrode is two orders of magnitude too slow to account for the observed deposition rate, suggesting that convection is involved. The onset of rapid deposition is accompanied by vigorous bubbling, which may induce convection currents and thus increase rate.

The spring surface texture, Figure 14, is likely due to stray current between the spring surface and the uninsulated Pt wire. Figure 15 shows that the spring has a hollow core. It is hollow only on one side, possibly due to an asymmetry in the electrode, where a sharp tip protrudes at right angles to the shaft. In open loop mode, deposition rate is faster than tip movement and thus the deposit tends to envelop the tip, which may result in a hollow interior. If this effect can be controlled it could be used to advantage.



**Figure 12 : Nickel Column (10 $\mu$ m diameter).**

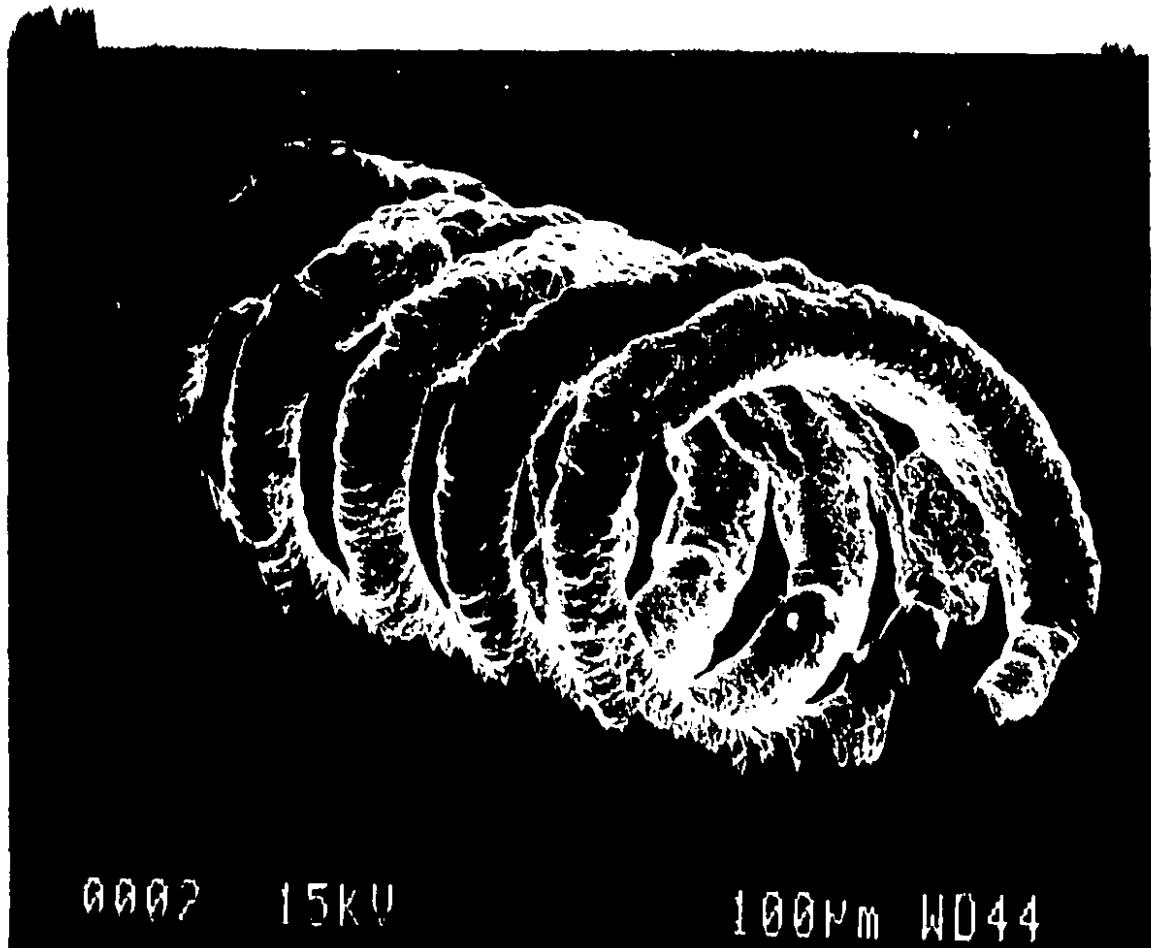


Figure 13 : Nickel Spring (1mm diameter).



Figure 14 : Surface of the Spring.



**Figure 15 :** Cross-Section of the Spring Loop,  
revealing a hollow interior.



**Figure 16 : Nickel Wall.**

It is possible to modify structures after they are built. A cross piece was electrodeposited onto a spring (not shown) so that forces could be applied along the axis of symmetry. The addition was made a week after the initial fabrication, and appeared to be mechanically robust, although no quantitative measurements were made.

Thus far work has concentrated on building columns and wires. The next stage is to construct walls and solids. Figure 16 shows the first attempt at building a wall. It is 60  $\mu\text{m}$  high, 500  $\mu\text{m}$  long and approximately 15  $\mu\text{m}$  wide. To build the wall the electrode tip was scanned horizontally, moving vertically in 3  $\mu\text{m}$  increments after each pass. In the process of building the wall, the tip tended to catch on the forming surface as deposit occasionally grew up to envelop it.

## **6.2 Material Properties**

### **6.2.1 Spring Constant and Modulus of Elasticity**

An estimate of the spring's modulus of elasticity was obtained from a measurement of the spring constant. A silicon beam force transducer (SensoNor AE801, Horten Norway) was mounted on a micro-stepping motor driven stage and lowered directly onto the spring in order to induce compression. Figure 17 is a plot of the measured force-displacement relationship.

The silicon beam contains two resistors which change dimensions as the beam deflects. One is compressed and the other expands, which in turn affects their resistances. The values of the resistances were measured as a function of displacement using two multimeters (an HP34401A and a Keithley 2001), from which the force on the beam was determined. A bridge circuit could be used to provide a more accurate measure of resistance, but given the large uncertainties in spring geometry and thus in the determination of the modulus of elasticity, such accuracy is unnecessary. The displacement values in Figure 17 are corrected for

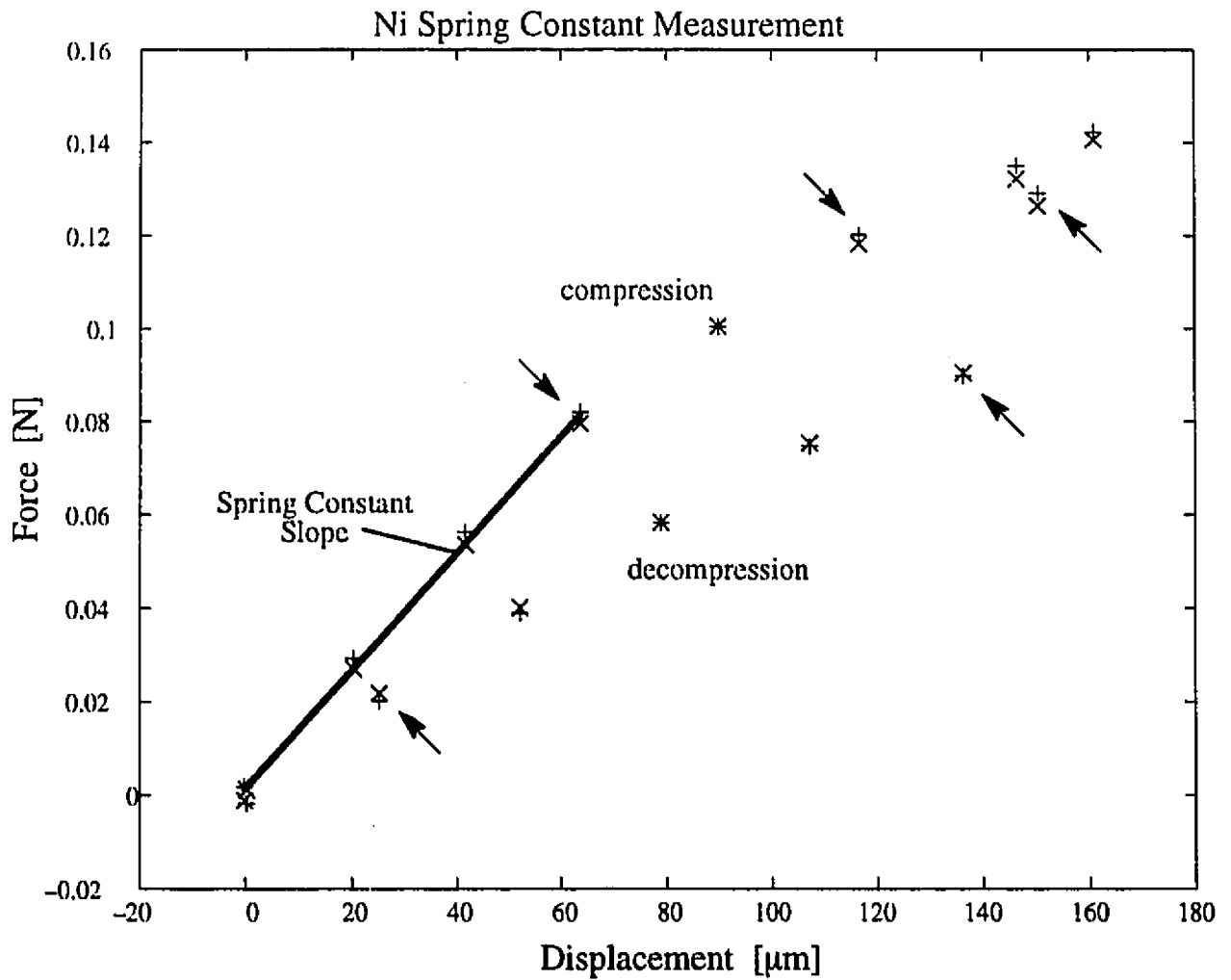


**Figure 17:** Measurement of the Spring Constant. Note the points where the slope changes abruptly due to slippage between the spring and the force transducer (indicated by arrows). The + s and  $\times$  s indicate values determined from the compressed and extended resistors on the Si beam transducer, respectively.

the deflection of the beam. The bending of the beam also resulted in the occasional sideways slippage of the spring relative to the beam, as indicated by arrows.

The spring constant was found to be 1.3 kN/m. Given the spring constant,  $k$ , wire diameter,  $d$ , number of turns,  $n$ , and spring radius,  $R$ , the shear modulus,  $G$ , is [104]:

$$G = \frac{64knR^3}{d^4} \quad (25)$$

Assuming that the material is polycrystalline and thus isotropic, the modulus of elasticity,  $E$ , is related to shear modulus and Poisson's ratio:

$$E = 2G(1 + \mu) \quad (26)$$

yielding a modulus of elasticity of  $240 \pm 120$  GPa. The large uncertainty in the result is due to uncertainty in the spring wire diameter, on which the modulus depends to the fourth power. An accepted value for the modulus of elasticity of nickel is 211 GPa [104].

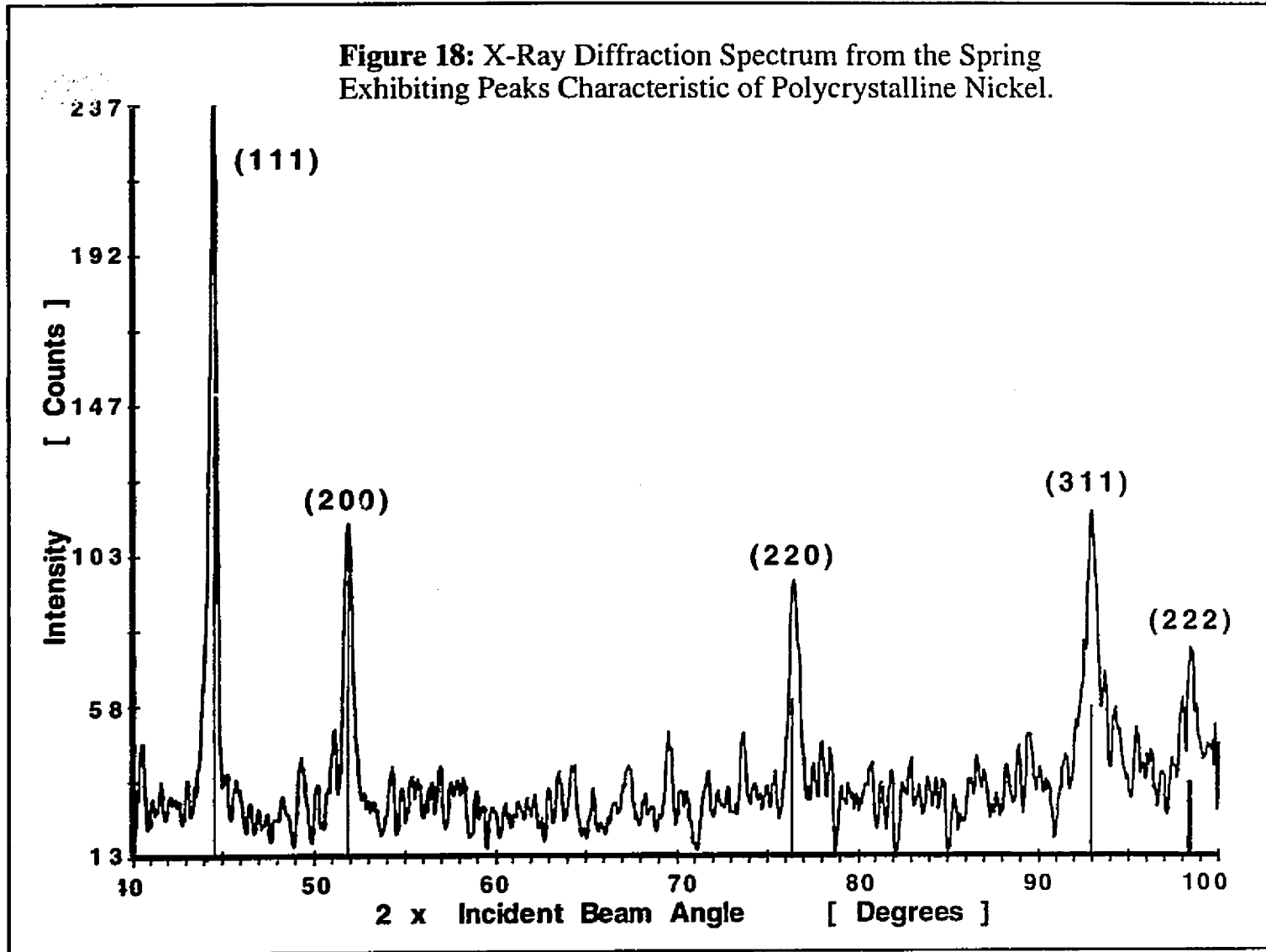
## 6.2.2 X-ray Crystallography

An x-ray diffraction spectrum, shown in Figure 18, demonstrates that the deposited material is in fact polycrystalline nickel. Copper  $\alpha$  monochromatic x-rays ( $\lambda = 154.178$  pm) probed the spring in a diffractometer (Rigaku RTP500RC). The spectral line angles,  $2\theta$ , in Figure 18 correspond to lines predicted by Bragg diffraction from nickel's face centered cubic (FCC) crystal planes, given by [105]:

$$\lambda = 2d \sin \theta \quad (27)$$

where  $d$  represents the plane spacing. In a cubic crystal  $d$  is given in terms of Miller ( $hkl$ ) indices and the lattice constant,  $a$ , by the relation:

**Figure 18: X-Ray Diffraction Spectrum from the Spring Exhibiting Peaks Characteristic of Polycrystalline Nickel.**



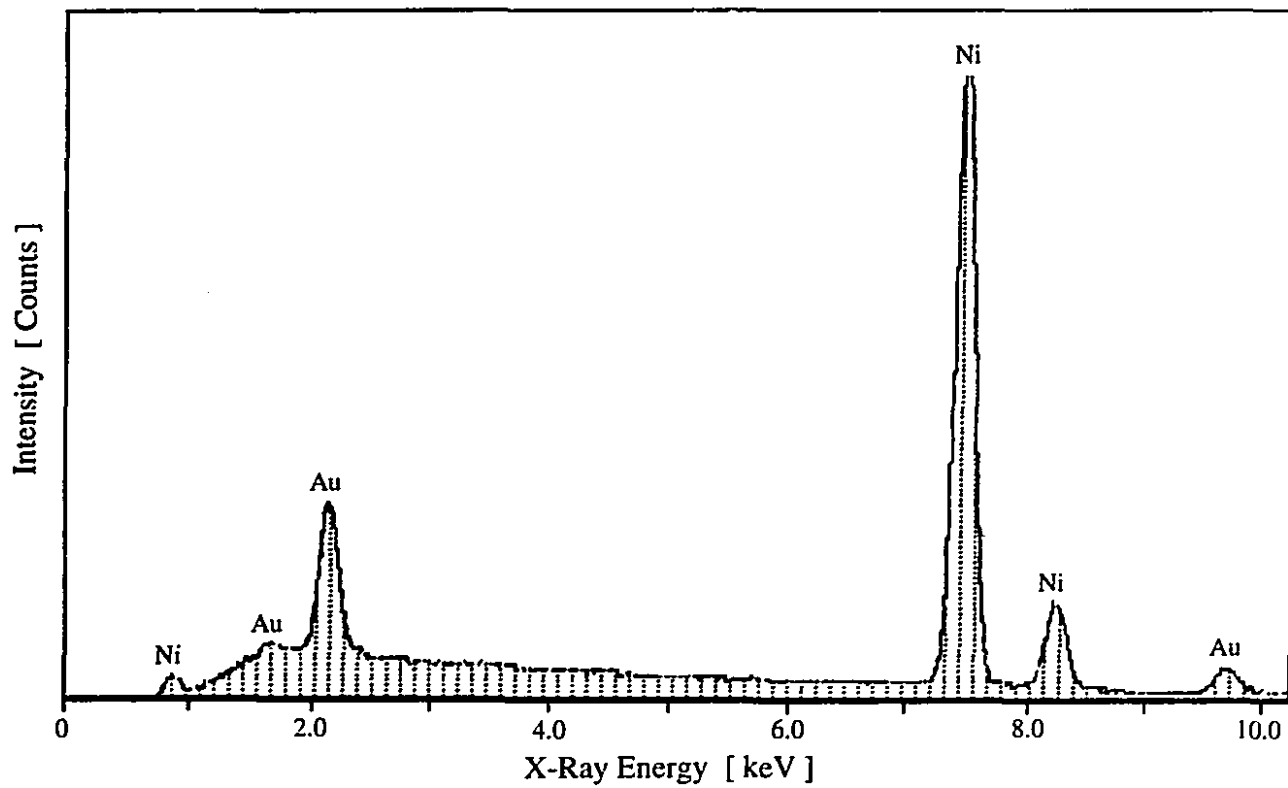


**Figure 19 :** X-ray Spectrum Emitted on Electron Bombardment of the Spring (Energy Dispersive X-ray Analysis), qualitatively demonstrating the presence of nickel and gold.

$$\frac{1}{d^2} = \frac{(h^2 + k^2 + l^2)}{a^2} \quad (28)$$

The lattice constant  $a=352.38$  pm for nickel at 20°C.

The x-ray results are confirmed by Energy Dispersive X-ray Analysis, Figure 19. In this process an electron beam excites x-ray emission in the probed material. The apparatus generally consists of an electron microscope fitted with an x-ray detector. Elements produce characteristic emission spectra, allowing their identification. The spectrum in Figure 19 demonstrates that the material is indeed nickel. No impurities are visible. The technique is sensitive to elements with molecular weights greater than oxygen and does not reveal crystal structure. The gold lines shown are due to a thin layer of gold evaporated onto the sample to improve electron microscope images.

### 6.3 Measuring Conductivity

As part of the effort towards developing a complete model of the electro-deposition process, the conductivity of the sulfamate solution was measured. The measurement procedure and the theory behind it also provide some insight into the nature of the electrode/electrolyte interface and transport mechanisms. They are thus presented in some detail.

#### 6.3.1 Theory

Electrolyte solutions are ohmic conductors, providing voltages are not too high. Conductivity depends on concentration, charge distribution, viscous drag (electrophoretic effect) and changes in the ionic atmosphere due to charge movement (relaxation effect). Such considerations lead to the Debye-Hückel-Onsager relation [87] relating molar conductivity,  $\Lambda_m$ , (the conductivity divided by electrolyte concentration) and concentration,  $C$ .

$$\Lambda_m = \Lambda_m^o - (A + B\Lambda_m^o) C^{1/2} \quad (29)$$

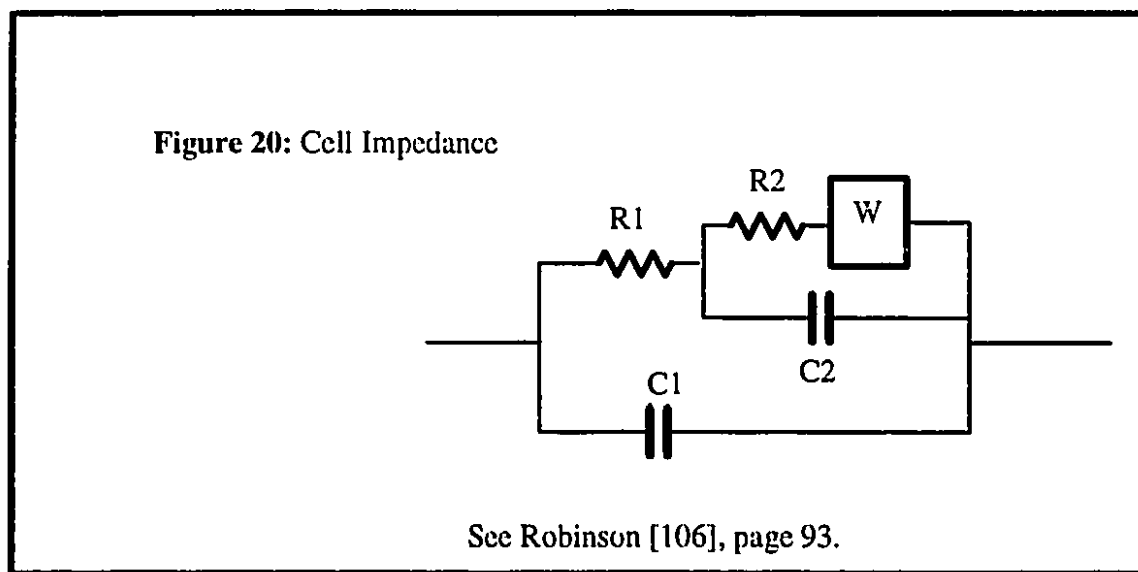
$A_m^o$  is the conductivity at infinite dilution.  $A$  and  $B$  are constants depending on ionic charge, geometry, the permittivity of the medium and the viscosity. The relation is good for strong electrolytes at low concentrations. However, in electrodeposition concentrations of greater than 1M are used in order to maximize plating rates. Such concentrations are beyond the model's effective range. Thus conductivity at a given concentration must be determined experimentally.

Conductivity,  $\kappa$ , is generally measured using a cell containing the solution and two electrodes. A voltage is applied and the current is measured. Resistance,  $R$ , is calculated using Ohm's Law. The relationship between conductivity and resistance depends on cell geometry. A solution of known conductivity,  $\kappa_s$ , is generally used to calibrate the cell [87][106]. The unknown conductivity is determined from  $R$ ,  $\kappa_s$ , and  $R_s$  (the calibration solution resistance) using the relation:

$$\kappa = \frac{R_s}{R} \kappa_s \quad (30)$$

Temperature and electrode polarization complicate the procedure [106]. Electrolyte conductivity changes by about  $2 \pm 0.5\% \text{ K}^{-1}$ . Polarization is the result of charge build-up at the electrodes. An impedance is produced in series with the electrolyte bulk resistance, Figure 20. The polarized region or double layer is modelled as a capacitance,  $C_2$ , in parallel with a resistance,  $R_2$ , and a non-linear impedance,  $W$ . The bulk electrolyte resistance,  $R_1$ , is shown in series with the double layer.  $C_1$  represents cell capacitance. Audio frequency alternating current is generally used as the cell input at frequencies where the double layer impedance becomes negligible relative to that of the bulk resistance. The effect of the double layer is further reduced by using electrodes made of a non-polarizable material such a platinum. When non-polarizable electrodes are used, frequencies in the kiloHertz range are suf-

ficient. At MegaHertz frequencies the Debye–Falkenhagen effect is produced, where the field is switched so rapidly that ions remain stationary, eliminating relaxation effects and reducing impedance. (Other effects, such as circuit inductance, must also be considered at such high frequencies.)



### 6.3.2 Apparatus and Procedure

An electrolytic cell was constructed, Figure 21. The cell is contained in a pyrex dish (depth 60 mm, length 230 mm, width 110 mm, not shown to scale in the figure). 400 mm<sup>2</sup> stainless steel electrodes (low polarizability) are epoxied to a Delrin base, spaced 100mm apart. The Delryn base is 10mm deep. Copper wires are soldered to the electrodes and covered with glass pipettes.

The cell was designed to have a bulk solution resistance on the order of a few ohms to allow potentials up to about 1 V to be applied by the impedance analyzer, and to ensure that bulk resistance is clearly distinguishable from double layer impedance at high audio frequencies. The cell capacitance was kept low (~10 nF) to avoid bypass of the bulk at high frequencies.

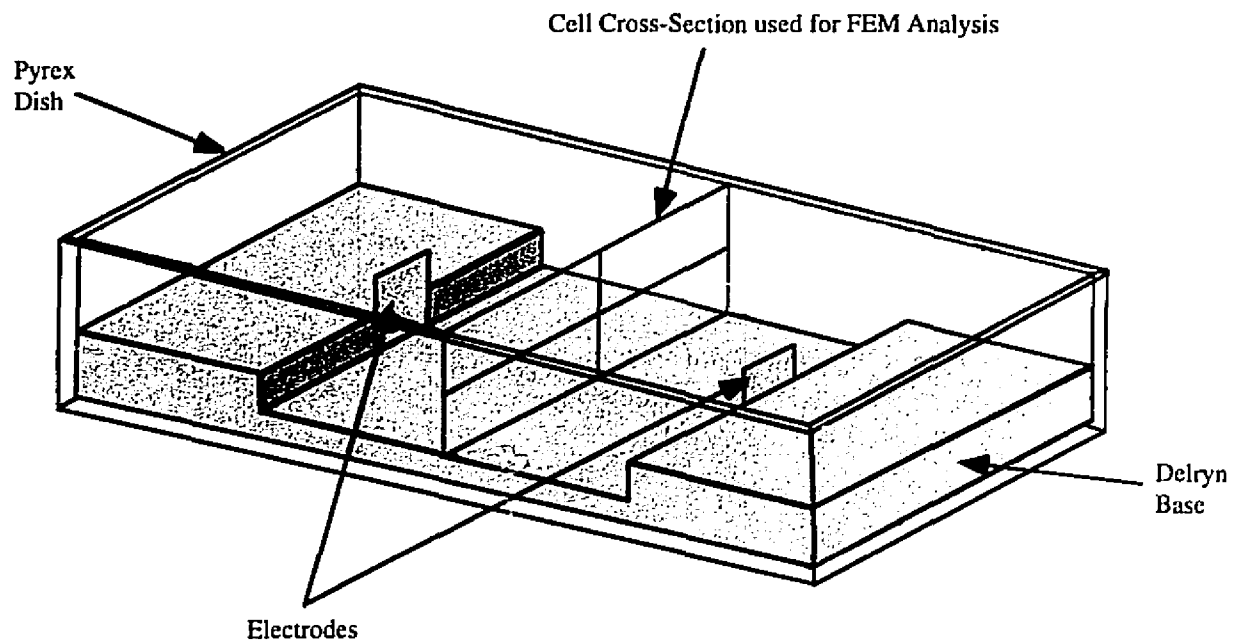


**Figure 21 :** Electrochemical Cell fabricated for Impedance Measurements.  
(Pyrex dish not to scale.)

The transparency of the apparatus allows visual inspection at all times. A 0.95 M KCl calibration solution and a sulfamate solution ( $\text{Ni}(\text{SO}_3\text{NH}_2)_2$  : 450 g/L,  $\text{H}_3\text{BO}_3$  : 30 g/L) were prepared.

Impedance was measured from 100 Hz to 40 MHz using an HP4194A Impedance Gain/Phase Analyzer. The bulk resistance was taken to be the magnitude of the impedance where the phase was zero and the magnitude was constant with frequency, as expected for a resistor.

Horizontal movement of the electrodes relative to the cell had no noticeable effect on measured impedance. Depth change, however, produced a significant effect. The removal of 100ml of solution altered the measured resistance by about 12%. Finite element modelling of the cell predicts relatively high current densities along the surface of the solution, suggesting that depth changes will affect resistance. Figure 21 shows the model geometry, including the location of the cross-section used for the current density results in Figure 22. Solution volumes were determined from graduations on the beakers used, accurate to only  $\pm 50$  ml. The uncertainty due to depth is estimated to be  $\pm 6\%$ . (While the uncertainty is quite large, the purpose of the experiment was simply to obtain an approximate value for future modelling of the system. More accurate measurements could be made by monitoring the solution volumes more carefully or by using a different cell geometry.)

A temperature of 22 °C was measured during the experiment. The experiment took place over three hours, over which time the temperature changed by  $< \pm 2$  °C. Given that electrolytes change in conductivity by about  $2\% \text{K}^{-1}$ , the resulting uncertainty is 4%. A calibration conductivity value for KCl of  $\kappa_s = 10.6 \pm 0.4 \text{ S/m}$  was found by interpolation between standard values for 0.95 M KCl at 18 and 25 °C. The error bounds account for the uncertainty in temperature.

The impedance of the standard KCl solution was measured, followed by that of the sulfamate solution. The KCl standard was then remeasured using fresh solution. All measurements were taken between 100 Hz and 10 MHz with a 1 V applied potential. An RLC

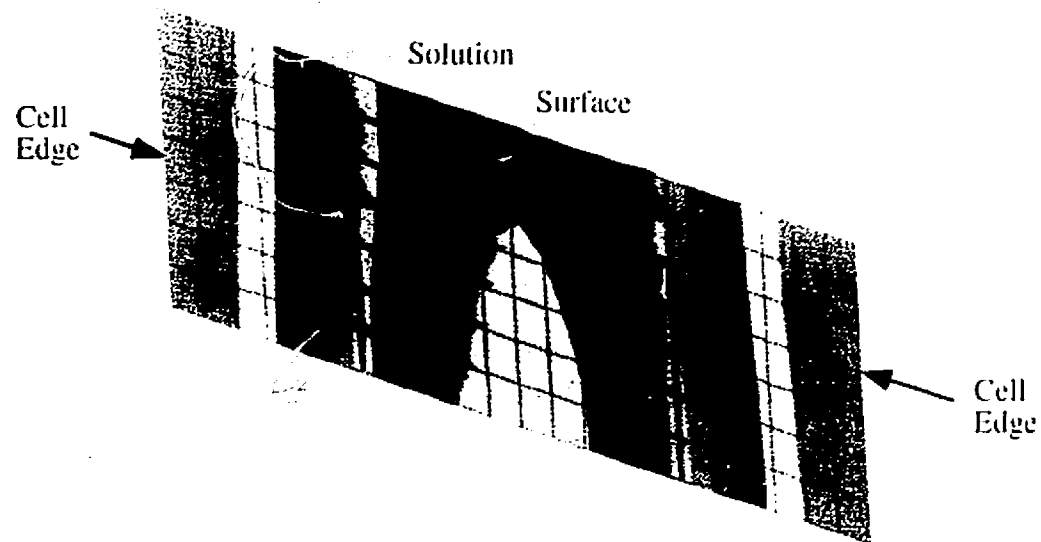


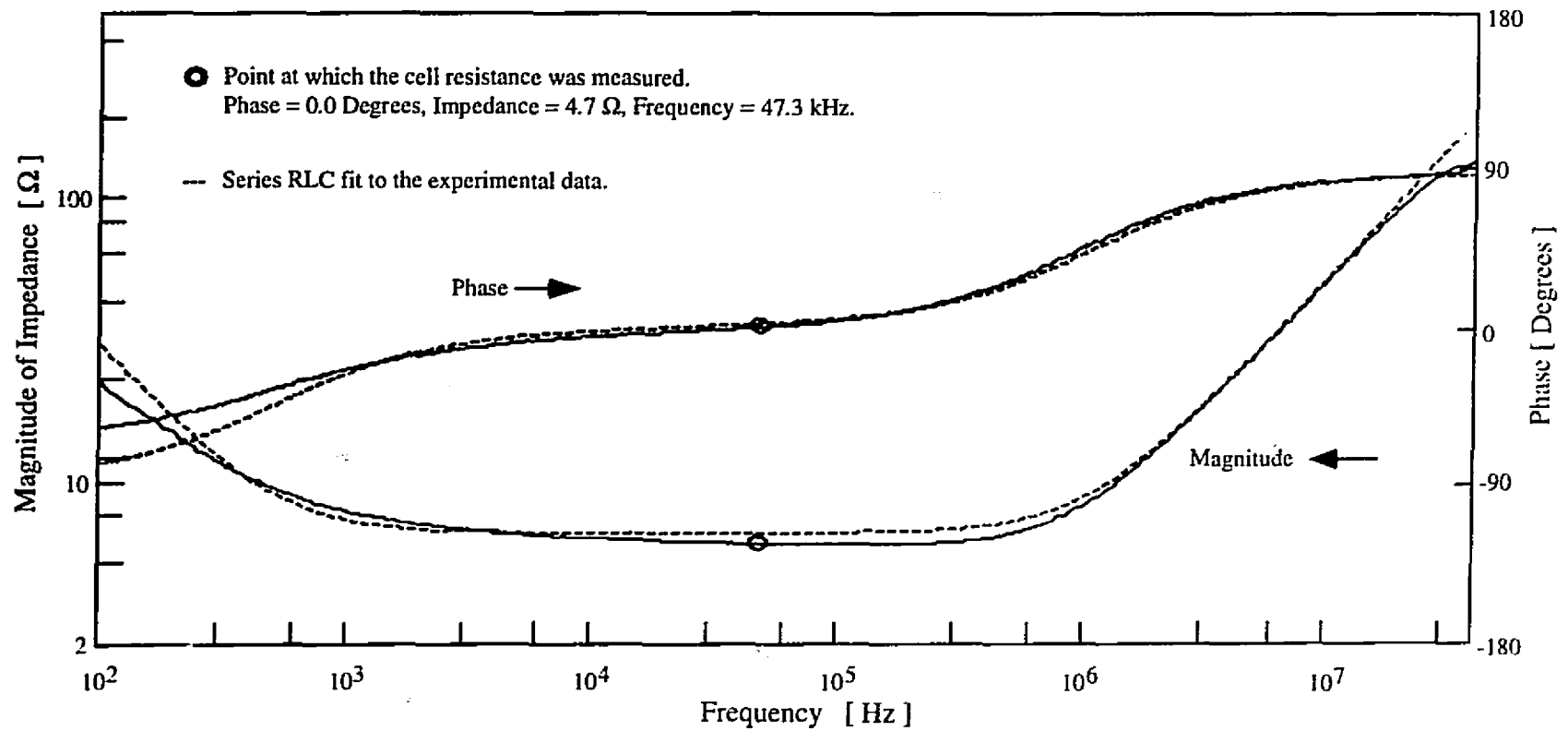
**Figure 22 :** Current Density between Electrodes in the Conductivity Cell, as predicted by finite element modelling, indicating that current at the solution surface is significant, and thus that solution depth is important to the conductivity measurement. Contours are linearly spaced, representing a variation in current density between the edges (low) and the center (high) of only 1.4 times. The cross-section taken is indicated in Figure 21.

circuit model was fit to the measured data. Bulk resistance was determined at frequencies of about 45 kHz, where the impedance was constant with respect to frequency and phase was zero.

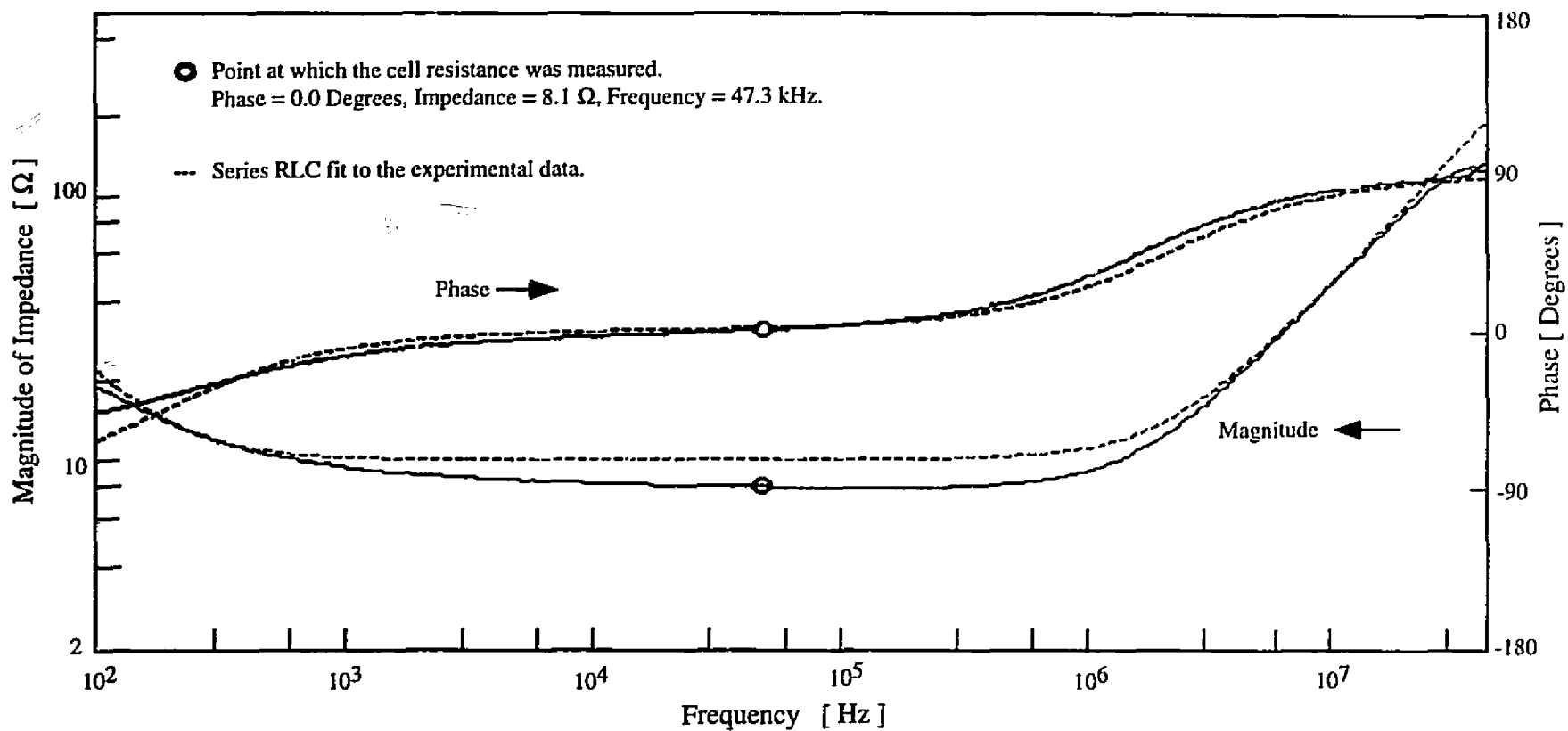
### 6.3.3 Results

Figure 23 and Figure 24 show measured impedance magnitude and phase as a function of log frequency. The dotted lines represent results from a least squares fit to the data of a resistance (R), an inductance (L) and a capacitance (C) in series. The double layer impedance,  $W$ , is often modelled as a series RC with an inverse square root frequency dependence [106], explaining the deviation of the RLC fit from the measured impedance. The conductivity of the sulfamate solution was found to be  $6.0 \pm 0.8$  S/m at 22°C.

**Figure 23 : Impedance of the Cell with the KCl Calibration Solution.**



**Figure 24 : Impedance of the Cell Containing Sulfamate Solution.**



## Chapter 7 : Discussion and Future Work

In Chapter 1, four requirements were made of a fabrication process, namely (1) a truly three dimensional fabrication capability, (2) sub-micrometer spatial resolution, (3) a range of suitable materials for the construction MEMS components and (4) reasonable fabrication rates. These were chosen to meet the laboratory need for a means of producing tools and end effectors for the micro-robots and micro-manipulators under development. A process or set of procedures satisfying the four general requirements could also be suitable for building a range of sub-millimeter sized artificial organisms, integrating mechanical structures, actuators, sensors, power sources and intelligence. As discussed in Chapter 2, no methods are currently available which satisfy these requirements.

The most widely used fabrication methods, based on photo-lithography and other micro-electronics technology, are restricted to the production of low aspect ratio, silicon and gallium arsenide structures. LIGA, an extension of photo-lithography, produces high aspect ratio moulds, allowing a variety of materials to be employed. Its main limitation is that it effectively "extrudes" a two dimensional pattern into 3D at the expense of features in the third dimension.

Excimer laser machining is the material removal process best suited to the requirements. It is capable of machining many materials including polymers, metals and ceramics at high rates ( $\sim 2.500 \mu\text{m/s}$ ) and with sub-micrometer resolution. Unfortunately high resolution is achieved at the expense of cut depth because of the high numerical apertures required to reduce focal volume. Also, as is generally the case with machining processes, assembly methods are needed. Current assembly technology is rather crude, a situation which will hopefully be rectified by the development of sophisticated micro-manipulators.

Several truly three dimensional micro-fabrication processes are under development. Laser enhanced chemical vapour deposition (LCVD), stereo lithography and spatially constrained micro-electrodeposition (SCMED) all have produced 3D structures with mi-

rometer scale resolutions (5 to 10 micrometers) at micrometer per second rates. Work presented in this thesis has brought SCMED to a level of development comparable to those of LCVD and stereo lithography. The construction of a spring demonstrates that SCMED is capable of producing three dimensional nickel structures on the micrometer scale. A spatial resolution of 10  $\mu\text{m}$  has been achieved and deposition rates of 6  $\mu\text{m/s}$  observed. X-ray diffraction results indicate that the deposited nickel is polycrystalline, while a measurement of the spring constant yields a modulus which agrees within experimental uncertainty with that expected for solid nickel. Once again, however, neither SCMED nor the other 3D technologies can yet meet the fabrication requirements. What are their prospects of achieving these aims?

LCVD and stereo lithography are currently limited in resolution by the laser wavelengths used, among other factors. Achieving sub-micrometer resolution would almost certainly involve the use of shorter wavelength sources (UVB, x-ray or electron beam) or near field objectives. Electron beams are only effective at low pressures, while short wavelength electromagnetic waves tend to have large penetration depths and may be too energetic to allow bonding. A version of LCVD using electron beams produces sub-micrometer resolution but at very low rates (20 nm/s). Both methods are also relatively restricted in the materials available, especially stereo lithography, which employs a mechanically poor polymer. The prospects of achieving sub-micrometer resolution and material diversity with either LCVD or stereo lithography while maintaining rapid deposition rates are unclear at best.

The potential of SCMED is much clearer. Two dimensional localized electrochemical deposition results (Section 2.3.6) demonstrate that metals can be electro-deposited with sub-micrometer resolution in two-dimensional patterns and that the deposition of polymers is also feasible. Many materials can be electrodeposited including pure metals, alloys and polymers. Electrochemical theory (Chapter 3) suggests that deposition rates may in fact increase as resolution is reduced. It remains to be shown, however, that complex three-dimensional micro-structures can be rapidly fabricated with sub-micrometer resolution using a

range of materials. Some of the obstacles to be overcome and ideas on how to tackle them are discussed in the remainder of this chapter.

## 7.1 Resolution

As discussed in Chapter 3, resolution is a function of field distribution. To improve resolution the field confinement must be improved. This can be done by reducing electrode tip dimensions. Efforts are focussing on the use of progressively sharper tips. STM and AFM tips have been produced with tip sizes of several nanometers. (Although these electrodes often end in a single atom, the very tip is often roughly hemispherical, with a diameter of  $\geq 50$  atoms.) Insulation of these tips is somewhat difficult. Electrodes have been dipped in glass [107], apiezon wax [108] and EpoxyLite [107]. Another approach is to evaporate insulating coatings such as SiO onto the electrodes, bring them close to a conducting surface and apply a high voltage to uncover the tip [78]. While it is difficult to control insulation such that the exposed electrode area is less than  $1 \mu\text{m}^2$ , the modelling presented in Chapter 3 demonstrates that a sharp tip alone will localize field. Insulation is only necessary to reduce background current so that the current can be used as feedback on tip to substrate separation. It may be that  $1 \mu\text{m}^2$  is a sufficiently small area to provide reasonable signal to noise for sub-micrometer deposition.

Three methods exist to characterize the shape of insulated tips. Ohmic resistance can be measured by applying kHz frequency signals [106], as was done in measuring solution resistance (Chapter 6). The resistance is then related to the tip surface area. Tip geometry is difficult to evaluate using this technique. The tip can also be examined under an electron microscope [107]. This requires gold coating, however, to reduce charging effects, so the tips are seldom re-used. Finally, the tip current – distance profile can be measured as a tip approaches a surface [75]. This gives information on both tip shape and the exposed area when the measurements are performed in a calibrated solution.

What is the ultimate resolution limit? This has yet to be fully investigated, but at some point the field will become so confined that no ions are present within it. If the solution concentration is 1 mol/L, the inter-ion distance is  $\approx 1$  nm. In a solid a typical atom spacing is on the order of 0.2 nm. Electrochemical etching, achieved by reversing the electrochemical potential, may turn out to produce higher resolution than deposition because it affects material in the solid state. Etching and subsequent re-deposition might also be possible.

Another issue determining resolution is the accuracy of tip positioning. A micro-fabrication robot being developed by Professor Ian Hunter's group in collaboration with MPB technologies offers 1 nm position accuracy over a workspace of several millimeters, and thus should be ideal for SCMED.

## 7.2 Control

The main difficulty with the present control system, in which contact between the tip and the growing surface is used to signal motion, is that deposition tends to occur around the tip. When lateral motions are made, as in building the wall (Section 6.1), the tip catches on the surface and structures are grown unevenly. In building the wall the electrode had to be manually tapped every few seconds to free it.

In order to improve the deposition control, A/Ds (VXI bus) are being installed to bring current feedback and other information to the workstation, allowing more sophisticated processing and feedback schemes to be devised. A digital I/O is also being installed to direct motor stepping, allowing greater flexibility and speed than are offered by the ASCII command based controllers.

Position feedback via tunneling current should be possible. The sharp electrodes used in SCMED are identical to the tips employed in scanning tunneling microscopy and tunneling currents have been measured in electrolytes (Section 2.3.6.3). Lowering the applied potential and periodically moving the tip into the tunneling range could be an effective means

of controlling tip to substrate distance.

### **7.3 Surface Finish**

Surface finish is affected by several factors including obstruction of the surface by bubbles, stray current (e.g. from the side of an uninsulated tip), motion of the tip relative to the surface and grain size. Several approaches could be used to improve surface finish, including improvement of tip position control, greater tip insulation and spatial low pass filtering of the surface by electro-polishing.

### **7.4 Materials**

The availability of a range of materials is particularly important because mechanical components, electronics, actuators, and sensors all have specific material requirements. The next stage of SCMED development involves the integration of actuators and electronics. It has already been demonstrated that nickel electro-deposits can be integrated with the nickel titanium artificial muscle fibers being developed in Professor Ian Hunter's laboratory [22]. The combination of SCMED structures with silicon microelectronics is promising since Ni can be grown directly on silicon substrates. Other materials which can be electro-deposited include many metals (Al, Au, Cd, Cr, Cu, Fe, In, Pb, Pt, Ag, Sn, and Zn are the most common), alloys (Brass, Bronze, Cd-Ti, Zn-Ni, Ag-Pb ...) [98] and conducting polymers.

Ultimately, it would be advantageous if a single material could be used to build an entire micro-electro-mechanical system. Conductive polymers such as polyaniline offer this possibility. Conductivity ranges over 11 orders of magnitude and can be readily switched, allowing transistors [109][110][111] and supercapacitors [112] to be built. The changes in oxidation state which affect conductivity also result in mechanical deformations which are being exploited to build actuators [20]. Chemical sensors [113][114] and LEDs [115] have also been built. Polyaniline composites can be imparted the tensile strength of Kevlar. There

is thus the potential to integrate mechanical, electrical, electromagnetic and chemical elements using one material. 2D localized deposition of polyaniline has already been achieved [82]. Experimenting with the three dimensional deposition of polyaniline is a priority for future work.

Finally, instrumentation must be set up and, in some cases, techniques developed to evaluate the material properties of micro-structures, including tensile strength, modulus of elasticity, hardness, life cycle, electromagnetic absorption and conductivity. Accurate results will often demand precise fabrication. Tests can be complemented by structural investigations. Electron microscopy and x-ray crystallography can reveal crystal structure, grain size and dislocation density, for example.

## **7.5 Underlying Mechanisms**

In order to understand the limitations of SCMED and to improve its performance it is important to determine the relative contributions of the various mechanisms involved in electrodeposition. In particular, it would be valuable to determine the mechanism of rate enhancement. The current hypothesis is that rate enhancement is due to convection induced by vigorous hydrogen release. Several factors make the study of a plating solution such as sulfamate difficult. Standard electrochemical testing procedures simplify analysis by using relatively low concentrations of reactants to eliminate migration effects and to allow the approximation that ion activity changes linearly with concentration. Electroplating solutions, on the other hand, are highly concentrated to permit maximum current density. Crystallization and evolution of bubbles further complicate analysis. In short, it is difficult to analyze electroplating and forming solutions under plating conditions. A thorough set of experiments needs to be devised which can distinguish the effects of each transport mechanism and those of electrode kinetics. A numerical model of the system would help predict the behaviors characteristics of the various mechanisms.

As discussed in Chapter 3, when tip dimensions are reduced, diffusion rates increase. This may enable high deposition rates to be achieved at potentials where bubble formation does not occur. The formation of bubbles likely roughens the deposit and may induce embrittlement as hydrogen diffuses into crystal dislocations [116].

Further experimentation should also be done to quantify the potential dependence of deposition rate and deposit quality. Knowledge of tip size and geometry (Section 7.1) should allow deposition profile and tip geometry to be related.

## **7.6 Machining and Alterations**

SCMED need not be restricted to a deposition mode. A fundamental feature of electrochemistry is that electrical potential can be varied to alter reaction kinetics and even reverse the reaction direction. The electrochemical potential can be set such that material is etched. SCMED is then a material deposition and removal process, and corrections or additions can be made. The ability to etch could be particularly valuable to separate deposits from the substrate.

## **7.7 A Micro-Fabrication Centre**

SCMED is the key technology in a micro-fabrication centre being assembled in Ian Hunter's laboratory. Other technologies in the centre include excimer and infra-red laser machining, glass, quartz and ceramic electrochemical machining, and wire electrical discharge machining. Manipulation and assembly are to be achieved using a micro-fabrication robot (MFR-1) and photon momentum. The goal is to create a centre capable of micro-depositing metals and polymers, micro-machining virtually all materials, and manipulating micro-structures such that MEMS can be constructed rapidly and effectively.

## Conclusion

The concept of localized electrochemical deposition has been demonstrated and nickel micro-structures built. Electrodeposition is spatially constrained by limiting the extent of the electric field which in turn localizes the deposit. Polycrystalline nickel is electrodeposited at rates two orders of magnitude faster than those of conventional electroforming, the rate enhancement likely the result of local convection induced by vigorous bubble formation. Fabricated structures include a multi-coiled helical spring and a 100 $\mu\text{m}$  high, 10 $\mu\text{m}$  diameter column. X-ray diffraction indicates that the material deposited is poly-crystalline nickel, while a measurement of the spring constant demonstrates that the modulus of elasticity corresponds to that of bulk polycrystalline nickel.

SCMED is capable of producing three dimensional structures at rapid deposition rates. It has yet to meet the two other design objectives of sub-micrometer resolution and the deposition of a variety of materials. However, results from two dimensional selective electrodeposition processes suggest that the three dimensional electro-deposition and etching of metals and conducting polymers with sub-micrometer spatial resolution is feasible. Prospects for achieving the design objectives, and thereby overcoming the serious limitations of current fabrication technology, are promising.

## References

- [1] R.P. Feynman, "There's Plenty of Room at the Bottom", *Engineering and Science*, 23(2), pp. 22–36, 1960.
- [2] W. Trimmer, *Integrated Micro–Motion Systems*, F. Harashima, ed., Amsterdam: Elsevier, pp. 1–19, 1990.
- [3] I.W. Hunter, S. Lafontaine, P.M.F. Nielsen, P.J. Hunter and J.M. Hollerbach, "Manipulation and Dynamic Mechanical Testing of Microscopic Objects Using a Tele–Micro–Robot System", *IEEE Control Systems*, vol. 10, pp. 3–9, 1990.
- [4] I.W. Hunter et. al., "A Teleoperated Microsurgical Robot and Associated Virtual Environment for Eye Surgery", *Prescence*, vol. 2, pp.265–280, 1993.
- [5] I.W. Hunter, J.D.Madden and S.R.Lafontaine, *Disclosure Document Number 332193 – Spatially Constrained Electro–Deposition*, Washington, U.S. Department of Commerce, May 1993.
- [6] S.D.Senturia, "Feynman Revisited", *Proceedings – IEEE Micro Electro Mechanical Systems*, pp.309–312, 1994.
- [7] K.E. Drexler, *Nano–systems: Molecular Machining, Manufacturing and Computation*, New York: Wiley, 1992.
- [8] H.Guckel, et. al., "A first Functional Current Excited Planar Rotational Magnetic Micro-motor", *Proceedings – IEEE Micro Electro Mechanical Systems*, pp.7–11, 1993.
- [9] D.M.Eigler and E.K.Schweizer, "Positioning of single atoms with a Scanning Tunneling Microscope", *Nature*, vol.344, pp.524–6, 1990.
- [10] B. Sarcosia et. al., "Chirality of the Local Supercoiling of Individual DNA Molecules assigned by Atomic Force Microscopy", *Proceedings of SPIE*, vol. 1855, pp.12–16, 1993.
- [11] G.Stix, "Micron Machinations", *Scientific American*, vol.267:5, pp.105–115, 1992.
- [12] J.Bryzek, K.Petersen and W.McCulley, "Micromachines on the March", *IEEE Spectrum*, pp.20–31, May, 1994.

- [13] L. Stryer, *Biochemistry: The Molecular Basis of Cell Structure and Function*, 3ed., New York: Freeman, 1988.
- [14] W.T. Keeton and J.L. Gould, *Biological Science*, 4th ed., New York: Norton, 1986.
- [15] A.L. Lehninger, *Biochemistry*, 2nd ed., New York: Worth, 1979.
- [16] P.Clark, "Cell and Neurone Growth Cone Behavior on Micro-patterned Surfaces", *Proceedings of the Nanofabrication and Biosystems Conference*, Cambridge: Cambridge Press, in press.
- [17] P.E.Hockberger, B.Lom, A.Sockarno and K.E.Healy, "Analysis of Neuronal Migration on Microfabricated Surfaces", *Proceedings of the Nanofabrication and Biosystems Conference*, Cambridge: Cambridge Press, in press.
- [18] A.Kawana, "Formation of a Simplified Model Brain on Microfabricated Electrode Arrays", *Proceedings of the Nanofabrication and Biosystems Conference*, Cambridge: Cambridge Press, in press.
- [19] A.A.Griffith, "The Phenomena of Rupture and Flow in Solids", *Philosophical Transactions of the Royal Society of London. Series A*, vol. 221, pp. 163-98, 1920.
- [20] E. Smela, O.Ingnas, I. Lundstrom, "Conducting Polymers as Artificial Muscles: Challenges and Possibilities", *Journal of Micromechanics and Microengineering*, vol. 3, pp. 203-5, 1993.
- [21] I.W. Hunter and S.Lafontaine, "A Comparison of Muscle with Artificial Actuators", *Technical Digest of the Fifth IEEE Workshop on Solid State Sensors and Actuators*, 5, pp.178-85, 1992.
- [22] S.R.Lafontaine, I.W.Hunter and L.A.Jones, "NiTi Artificial Muscle Fibers for Micro-Robotics and Medical Applications", *Proceedings - Industrial Applications of Shape Memory Alloys*, Quebec City, August, 1994.
- [23] C.F. Coombs, *Printed Circuits Handbook*, 2ed. New York: McGraw Hill, 1979.
- [24] *Proceedings - IEEE Micro Electro Mechanical Systems*, M.Esashi ed., Oiso, Japan, February, 1994.

- [25] Gianchandani, Y and Najafi, K., "Batch Fabrication and Assembly of Micromotor-Driven Mechanisms with Multi-Level Linkages", *Proceedings – IEEE Micro Electro Mechanical Systems*, pp.141–146, 1992.
- [26] W. Trimmer and R. Jebens, "Harmonic Electrostatic Motors", *Sensors and Actuators*, Vol. 20, pp. 17–24, 1989.
- [27] W.Ehrfeld, M.Abraham, U.Ehrfeld, M.Lacher and H.Lehr, "Materials for LIGA", *Proceedings – IEEE Micro Electro Mechanical Systems*, pp.86–90, 1994.
- [28] P.B.Fischer and S.Y.Chou, "10nm Electron Beam Lithography and sub–50nm Overlay using a Modified Scanning Electron Microscope" *Applied Physics Letters*, vol. 62, pp.2989–91, 1993.
- [29] F.B.Fischer and S.Y.Chou, "Sub–50nm High Aspect–ratio Silicon Pillars, Ridges, and Trenches Fabricated using Ultra–high Resolution Electron Beam Lithography and Reactive Ion Etching", *Applied Physics Letters*, vol. 62, pp.1414–16, 1993.
- [30] A. Franks, "Nanotechnology", *Journal of Physics E: Scientific Instrumentation*, vol. 20, pp.1442–51, 1987.
- [31] T.H.P.Chang et.al., "Nanostructure Technology", *IBM Journal of Research and Development*, vol. 32, 1988.
- [32] A.B. Frazier and M.G. Allen, "High Aspect Ratio Microstructures Using a Photosensitive Polyimide Process" *Proceedings – IEEE Micro Electro Mechanical Systems*, p.87–92, 1992.
- [33] M.Mehregany, S.F. Bart, L.S. Tavrow, J.H. Lang, S.D. Senturia and M.F. Schlecht, "A Study of Three Microfabricated Variable Capacitance Motors", *Sensors and Actuators*, A21–3, pp.173–9, 1990.
- [34] M.W.Judy and R.T.Howe, "Polysilicon Hollow Beam Resonators", *Proceedings – IEEE Micro Electro Mechanical Systems*, p.265–271, 1993.
- [35] A.Rogner, J.Eicher, D.Münchmeyer, R–P.Peters and J.Mohr, "The LIGA Technique – What are the New Opportunities", *Journal of Micromechanics and Microengineering*, vol.

2, pp.133–140, 1992.

[36] H.C.Ahn and M.G.Allen. "A Fully Integrated Micromachined Magnetic Particle Manipulator and Separator", pp.91–96, 1994.

[37] M. Harmening et. al. "Moulding of Three Dimensional Microstructures by the LIGA Process", *Proceedings – IEEE Micro Electro Mechanical Systems*, pp. 202–207, 1992.

[38] H. Guckel, T.R. Christenson, K.J. Skrobis, T.S. Jung, J. Klein, K.V. Hartojo, and I. Widjaja, "A First Functional Current Excited Planar Rotational Magnetic Micromotor", *Proceedings – IEEE Micro Electro Mechanical Systems*, pp.7–11 (1993).

[39] J.Mohr,P.Bley,M.Strohmann and U.Wallrabe, "Microactuators Fabricated by the LIGA Process", *Journal of Micromechanics and Microengineering*, vol. 2, pp.234–41, 1992.

[40] G.Schukov and A.Smith, "Micromachining with Excimer Lasers", *Lasers and Optonics*, vol. 9, pp.75–77, 1988.

[41] G.Poulin, G.Darcy and P.Eisele, "A Versatile Excimer Laser Processing System", *SPIE*, vol.998, pp.17–23, 1988.

[42] J.M.Hagerhorst and M.M.Oprysko, "Focussed Excimer Laser Beams: A Technique for Selective Micropatterning", *SPIE*, vol. 998, pp.105–112, 1988.

[43] L.S. Van Dyke, C.J. Brumlik and C.R. Martin, "UV Laser Ablation of Electronically Conductive Polymers" *Synthetic Metals*, vol. 52 pp.299–304 1992.

[44] R. Dizon, H. Han and M.L. Reed, "Single–Mask Processing of Micromechanical Piercing Structures Using Ion Milling", *Proceedings – IEEE Micro Electro Mechanical Systems*, pp.48–52, 1993.

[45] L.–M.Buchmann et.al., "Lithography with High Depth of Focus by an Ion Projection System", *Proceedings – Micro Electro Mechanical Systems*, pp.67–71, Travemünde, Germany, 1992.

[46] Y.Hatamura, M.Nakao, T.Sato, K.Koyano, K.Ichiki and H.Sangu, "Construction of 3–D Micro Structure by Multi–Face FAB Co–focus Rotational Robot and Various Mechani-

- cal Tools", *Proceedings – Micro Electro Mechanical Systems*, pp.297–302, 1994.
- [47] R.Germann, "Principles of materials Etching", *Nanofabrication and Biosystems*, Cambridge: Cambridge Press, In Press.
- [48] C.J. Humphreys, I.G. Salisbury, S.D. Berger, R.S. Timsit and M.E. Mochel, "Nanometer-scale Electron Beam Lithography", *Electron Microscopy and Analysis* (International Physics Conference Series 78), pp.1–6, 1985.
- [49] G.S.Chen, B.B.Boothroyd and C.J.Humphreys, "Novel Fabrication method for Nanometer-scale Silicon Dots and Wires", *Applied Physics Letters*, vol.62, pp. 1949–51, 1993
- [50] S.F.Krar et.al. *Technology of Machine Tools*, 2ed., New York : McGraw–Hill, 1976.
- [51] C.–L Kuo, T. Masuzawa and M. Fujino, "High Precision Micronozzle Fabrication" *Proceedings – IEEE Micro Electro Mechanical Systems*, pp.116–121, 1992.
- [52] K. Ikuta and K. Hirowatari, "Real Three Dimensional Fabrication Using Stereo Lithography and Metal Moulding" *Proceedings – IEEE Micro Electro Mechanical Systems*, pp. 42–47, (1993).
- [53] K.Ikuta, K.Hirowatari and T.Ogata, "Three Dimensional Micro Integrated Fluid Systems (MIFS) Fabricated by Stereo Lithography", pp.1–6, 1994.
- [54] E. Sachs, M. Cima, J.Bredt, A. Curodeau, T. Fan and D. Brancazio, "CAD–casting: direct fabrication of Ceramic shells and cores by Three Dimensional Printing", *Manufacturing Review*, vol. 5, pp. 117–26, 1992.
- [55] H. Westberg, M. Boman, S. Johansson and J. Schweitz, "Truly three dimensional Structures Microfabricated by Laser Chemical Processing", *Proceedings of Transducers 1991*, p.516, San Francisco, 1991.
- [56] F.T. Wallenberger and M. Boman, "Inorganic Fibers and Microstructures Directly from the Vapour Phase" *Composites Science and Technology* vol. 51, pp. 193–212, (1994).
- [57] M. Boman and H. Westberg, "Helical Microstructures Grown by Laser Assisted Chemical Vapour Deposition", *Proceedings – IEEE Micro Electro Mechanical Systems*, pp. 162–167, 1992.

- [58] S.Maeda, K.Minami and M.Esashi. "KrF Excimer Laser Induced Selective Non-Planar Metallization", *Proceedings of the IEEE Micro Electro Mechanical Systems*, pp.75-80, Oiso, Japan, 1994.
- [59] W.H.Brünger and K.T.Kohlmann. "E-beam Induced Fabrication of Microstructures", *Proceedings - Micro Electro Mechanical Systems*, pp.168-170, Travemünde, Germany, 1992.
- [60] G.Binnig, H.Rohrer, Ch.Gerber, and E.Weibel, " $7 \times 7$  Reconstruction on Si(111) Resolved in Real Space", *Physics Review Letters*, vol. 49, pp.57-61, 1983.
- [61] G.Binnig and H.Rohrer, "Scanning Tunneling Microscopy", *IBM Journal of Research and Development*, vol. 30, pp. 355-69, 1986.
- [62] D.W. Abraham, H.J.Mamim, E.Ganz and J.Clarke, "Surface Modification with the Scanning Tunneling Microscope", *IBM Journal of Research and Development*, vol. 30, pp.492-499, 1986.
- [63] R.L. McCarley, S.A.Hendricks and A.J.Bard, "Controlled Nanofabrication of Highly Oriented Pyrolytic Graphite with the Scanning Tunneling Microscope", *Journal of Physical Chemistry*, vol. 96, pp.10089-10092, 1992.
- [64] Y.-T.Kim and A.J.Bard, "Imaging and Etching of Self-Assembled n-Octadecanethiol Layers on Gold with the Scanning Tunneling Microscope", *Langmuir*, vol. 8, pp.1096-102, 1992.
- [65] J.A.Stroszcio and D.M.Eigler, "Atomic and Molecular Manipulation with the Scanning Tunneling Microscope", *Science*, vol. 254, pp.319-26, 1991.
- [66] D.M.Eigler and E.K.Schweizer, "Positioning of Single Atoms with a Scanning Tunneling Microscope", *Nature*, vol. 344, pp.524-6, 1990.
- [67] M. Parameswaran, D. Xie and P.G. Glavina, "Fabrication of Nickel Micromechanical Structures using a Simple Low Temperature Electroless Plating Process", *Journal of the Electrochemical Society*, Vol 140, pp. L111-14 1993.
- [68] C.H.Ting and M.Paunovic, "Selective Electroless Metal Deposition for Integrated Cir-

- cuit Fabrication", *Journal of the Electrochemical Society*, vol. 136, pp.456-62, 1989.
- [69] *Canning Handbook on Electroplating*, Birmingham:W. Canning Ltd., 1978.
- [70] R.J. von Gutfeld, R.E. Acosta and L.T. Romankiw, "Laser-Enhanced Plating and Etching: Mechanisms and Applications", *IBM Journal of Research and Development*, Vol. 26, pp.136-144 (1982).
- [71] J.Cl. Puippe, R.E. Acosta and R.J. von Gutfelt, "Investigation of Laser-Enhanced Electroplating Mechanisms", *Journal of the Electrochemical Society: Electrochemical Science and Technology*, Vol. 128, pp.2539-2545 (1981).
- [72] R.J.von Gutfeld, "Laser Enhanced Plating and Etching: Pyrolytic Effects", *Laser Processing of Integrated Circuits and Microelectronic Materials*, New York: Academic, pp.50-58, 1984.
- [73] A.J.Bard, F.-R.F.Fan, J.Kwak and O.Lev, "Scanning Electrochemical Microscopy. Introduction and Principles", *Analytical Chemistry*, vol. 61, pp.132-138, 1989.
- [74] R.Sonnenfeld and P.K.Hansma, "Tunneling in an Electrochemical Environment", *Science*, vol. 232, pp.211-16, 1986.
- [75] M.V. Mirkin, F.-R.F. Ren and A.J. Bard, "Scanning Electrochemical Microscopy Part 13. Evaluation of the Tip Shapes of Nanometer Size Microelectrodes", *Journal of Electroanalytical Chemistry*, vol 328, pp.47-62, 1992.
- [76] M.V.Mirkin and A.J.Bard, "Scanning Electrochemical Microscopy 18: Thin Layer Cell Formation with a Mercury Pool Substrate", *Journal of the Electrochemical Society*, vol.139, pp.3535-9, 1992.
- [77] C.W.Lin, F.-R.F.Fan and A.J.Bard, "High Resolution Photoelectrochemical Etching of n-GaAs with the Scanning Electrochemical and Tunneling Microscope", *Journal of the Electrochemical Society*, vol.134, pp.1038-9, 1987.
- [78] J. Schneir, P.K. Hansma, V. Elings, J. Gurley, K. Wickramasinghe and R. Sonnenfeld, "Creating and Observing Surface Features with a Scanning Tunneling Microscope", *SPIE* vol. 897, pp.16-19, 1988.

- [79] D.H.Craston and A.J.Bard, "High Resolution Deposition of Silver in Nafion Films with the Scanning Tunneling Microscope", *Journal of the Electrochemical Society*, vol.135, pp.785-6, 1988.
- [80] O.E.Husser, D.H.Craston and A.J.Bard, "Scanning Electrochemical Microscopy: High-Resolution Deposition and Etching of Metals", *Journal of the Electrochemical Society*, vol.136, pp.3222-9, 1989.
- [81] O.E.Husser, D.H.Craston and A.J.Bard, "High-Resolution Deposition and Etching of Metals with the Scanning Electrochemical Microscopy", *Journal of Vacuum Science and Technology*, vol.B6, pp.1873-6, 1988.
- [82] Y.-M. Wu, F.-R.F. Fan and A.J. Bard, "High Resolution Deposition of Polyaniline on Pt with the Scanning Electrochemical Microscope", *Journal of the Electrochemical Society*, vol. 136, pp. 885-6 1989.
- [83] A.A. Gewirth, D.H. Craston and A.J. Bard, "Fabrication and Characterization of Microtips for in situ Scanning Tunneling Microscopy", *Journal of Electroanalytical Chemistry*, vol.261, pp. 477-482, 1989.
- [84] J.D.Madden and I.W.Hunter, "3D Micro-Fabrication by Localized Electrochemical Deposition", *Journal of Microelectromechanical Systems*, submitted 1994.
- [85] Southampton Electrochemistry Group, *Instrumental Methods in Electrochemistry*, New York:Wiley, 1985.
- [86] A.J. Bard and R. Faulkner, *Electrochemical Methods: Fundamentals and Applications*, New York: Wiley, 1980.
- [87] P.W. Atkins, *Physical Chemistry*, 4th ed. New York:Freeman, 1990.
- [88] F.A. Lowenheim, *Electroplating*, McGraw Hill:New York, 1978.
- [89] R.M. Wightman and D.O. Wipf, "Voltammetry at Ultramicroelectrodes", *Electroanalytical Chemistry*, Vol. 15, p.267-353 (1989).
- [91] E. Raub and K. Muller, *Fundamentals of Metal Deposition*, New York:Elsevier, p.46, 1967.

- [92] J.D. Jackson, *Classical Electrodynamics*, 2nd ed., New York:Wiley, 1975.
- [93] M. Fotino, "Tip Sharpening by Normal and Reverse Electrochemical Etching", *Review of Scientific Instruments*, Vol. 64, pp. 159–167 (1993).
- [94] A.A. Gewirth, D.H. Craston and A.J. Bard, "Fabrication and Characterization of Micro-tips for in situ Scanning Tunneling Microscopy", *Journal of Electroanalytical Chemistry*, vol.261, pp. 477–482, 1989.
- [95] M.V. Mirkin, F.-R.F. Ren and A.J. Bard, "Scanning Electrochemical Microscopy Part 13. Evaluation of the Tip Shapes of Nanometer Size Microelectrodes", *Journal of Electroanalytical Chemistry*, vol 328, pp.47–62, (1992).
- [96] J.R. Brauer and B.E. MacNeal, *MSC EMAS User's Manual*, MacNeal-Schwendler Corp., 1991.
- [97] K.T.Brown and D.G.Flaming, "New Microelectrode Techniques for Intra-cellular Work in Small Cells", *Neuroscience*, vol. 2, pp.813–827, 1977.
- [98] F.A.Lowenheim, *Modern Electroplating*, 2ed., New York:Wiley, 1963.
- [99] S.Shoji and M.Esashi, "Photoetching and Electrochemical Discharge Drilling of Pyrex Glass", *Technical Digest of the 9th Sensor Symposium*, pp.27–30, 1990.
- [100] H.Kamada, H.Daiku and H.Maehata, "A Study on Machining of Ceramics Using Electro-Chemical Discharge", *Technical Report: Institute of Technology, Hitachi Zohsen*, vol. 47, No.3/4, pp. 16–22, 1986.
- [101] G.K.Batchelor, *An Introduction to Fluid Dynamics*, Cambridge: Cambridge University Press, 1967.
- [102] F.M.White, *Fluid Mechanics*, 2nd. ed., New York: McGraw Hill, 1986.
- [103] G. Petzow, *Metalloraphic Etching*, New York: American Society for Metals, p.45, 1978.
- [104] T. Baumeister ed., *Mark's Handbook*, 8th ed., McGraw-Hill, 1979.
- [105] B.D. Cullity, *Elements of X-ray Diffraction*, Reading Massachusetts: Addison-Wesley, pp. 96–102, 1956.

- [106] R.A.Robinson, *Electrolyte Solutions*, 2ed., London: Butterworths, 1959.
- [107] M.J.Heben, M.M.Dovek, N.S.Lewis,R.M.Penner and C.F.Quate, "Preparation of STM Tips for in-situ Characterization of Electrode Surfaces", *Journal of Microscopy*, vol. 152, pp.651-62, 1988.
- [108] L.A.Nagahara, T.Thundat and S.M.Lindsay, "Preparation and Characterization of STM tips for Electrochemical Studies", *Review of Scientific Instruments*, volume 60, pp.3128-30, 1989.
- [109] E.T. Jones, O.M. Chyan, and M.S. Wrighton, "Preparation and Characterization of Molecule-Based Transistors with a 50nm Source-Drain Separation with use of Shadow Deposition Techniques: Towards Faster, More Sensitive Molecule-Based Devices" *Journal of the American Chemical Society*, vol. 109, pp.5526-28, (1987).
- [110] E.P.Lofton, J.W.Thackeray and M.S.Wrighton, "Amplification of Electrical Signals with Molecule-Based Transistors: Power Amplification up to a KiloHertz Frequency and Factors Limiting Higher Frequency Operation", *Journal of Physical Chemistry*, vol. 90, pp.6080-83, 1986.
- [111] S.Chao and M.S.Wrighton, "Characterization of a Solid-State Polyaniline-Based Transistor: Water Vapour Dependant Characteristics of a Device Employing a Poly(vinyl alcohol)/Phosphoric Acid Solid-State Electrolyte", *Journal of the American Chemical Society*, vol. 109, pp.6627-31, 1987.
- [112] S.-C.Huang, S.-M.Huang, H.Ng, R.B.Kaner, "Polyaniline Capacitors", *Synthetic Metals*, 55-57, pp.4047-52, 1993.
- NO TAG E.Smela, O.Inganas and I.Lundstrom, "Conducting Polymers as Artificial Muscles: Challenges and Possibilities", *Journal of Micromechanics and Microengineering*, vol. 3, pp.203-5, 1993.
- [113] S.A.Krutovtsev, S.I.Sorokin, A.V.Zorin, Y.A.Letuchy and O.Y.Antonova, "Polymer Film-Based Sensors for Ammonia Detection", *Sensors and Actuators B [Chemical]*, vol. B7, pp.492-4, 1992.

[114] J.W.Thackeray, H.S.White and M.S.Wrighton, "Resistance of Polyaniline Films as a function of Electrochemical Potential and the Fabrication of Polyaniline-Based Microelectronic Devices", *Journal of Physical Chemistry*, vol. 89, pp.1441-7, 1985.

[115] G.Gustafsson, G.M.Treacy, Y.Cao, F.Klavetter, N.Colaneri and A.J.Heeger, "Flexible Light-Emitting Diodes made from Soluble Conducting Polymers", *Nature*, vol. 357, pp.477-479.

[116] T.H. Courtney, *Mechanical Behavior of Materials*, New York: McGraw-Hill, 1990.